The endoplasmic reticulum Ca^{2+}-ATPase SERCA2b is upregulated in activated microglia and its inhibition causes opposite effects on migration and phagocytosis

Running title: SERCA2b in microglial functions

Juan M. Morales-Ropero[1], Sandra Arroyo-Urea[1], Veronika E. Neubrand[1], David Martín-Oliva[1], José L. Marín-Teva[1], Miguel A. Cuadros[1], Peter Vangheluwe[2], Julio Navascués[1], Ana M. Mata[3], M. Rosario Sepúlveda[1#].

[1] Department of Cell Biology, Faculty of Sciences, University of Granada, Granada, Spain

[2] Laboratory of Cellular Transport Systems, Department of Cellular and Molecular Medicine, KU Leuven, Leuven, Belgium

[3] Department of Biochemistry and Molecular Biology and Genetics, Faculty of Sciences, University of Extremadura, Badajoz, Spain

[#] **Corresponding author:** M. Rosario Sepúlveda. Department of Cell Biology, Faculty of Sciences, University of Granada. Avda. Fuentenueva s/n, 18151, Granada, Spain. Tel. +34 958 246334, mrsepulveda@ugr.es

Abstract

Activation of microglia is an early immune response to damage in the brain. Although a key role for Ca^{2+} as trigger of microglial activation has been considered, little is known about the molecular scenario for regulating Ca^{2+} homeostasis in these cells. Taking into account the importance of the endoplasmic reticulum as a cellular Ca^{2+} store, the sarco(endo)plasmic reticulum Ca^{2+}-ATPase (SERCA2b) is an interesting target to modulate intracellular Ca^{2+} dynamics. We found upregulation of SERCA2b in activated microglia of human brain with Alzheimer´s disease and we further studied the participation of SERCA2b in microglial functions by using the BV2 murine microglial cell line and primary microglia isolated from mouse brain. To trigger microglia activation, we used the bacterial lipopolysaccharide (LPS), which is known to induce an increase of cytosolic Ca^{2+}. Our results showed an upregulated expression of SERCA2b in LPS-induced activated microglia likely associated to an attempt to restore the increased cytosolic Ca^{2+} concentration. We analyzed SERCA2b contribution in microglial migration by using the specific SERCA inhibitor thapsigargin in scratch assays. Microglial migration was strongly stimulated with thapsigargin, even more than with LPS-induction, but delayed in time. However, phagocytic capacity of microglia was blocked in the presence of the SERCA inhibitor, indicating the importance of a tight control of cytosolic Ca^{2+} in these processes. All together, these results provide for the first time compelling evidence for SERCA2b as a major player regulating microglial functions, affecting migration and phagocytosis in an opposite manner.

Keywords: Calcium pump, endoplasmic reticulum, microglia, brain, migration, phagocytosis, Alzheimer´s disease.

Main points:

- SERCA2b is upregulated in activated microglia *in vitro* and in Alzheimer´s disease-affected brains.
- SERCA2b inhibition stimulates migration but prevents phagocytosis in microglia.

Table of Contents Image:

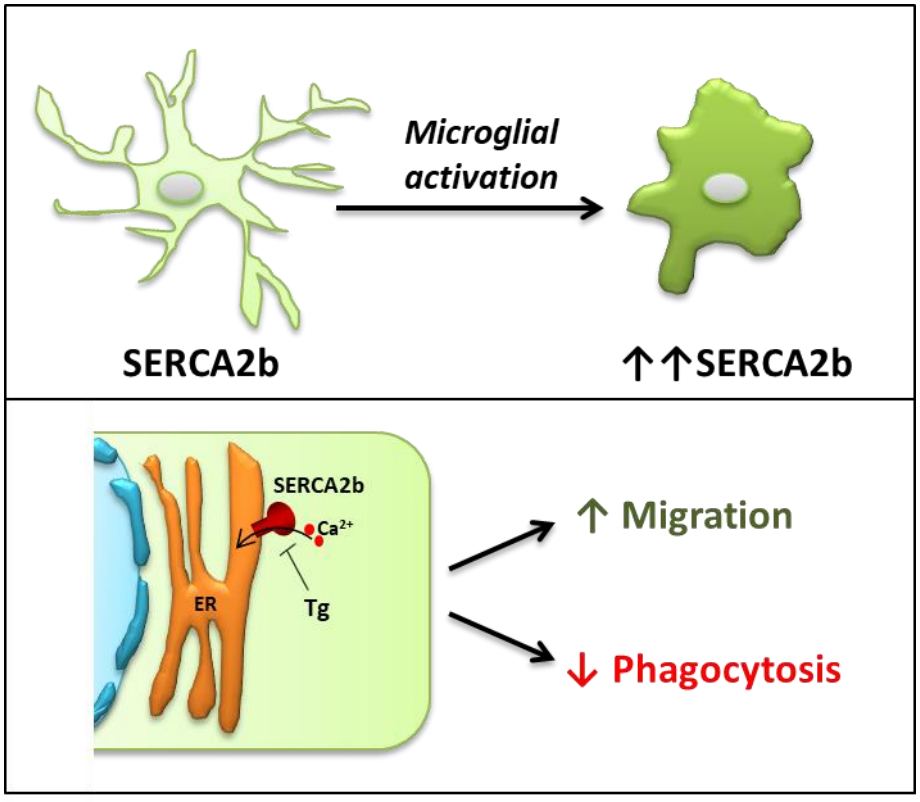

1. INTRODUCTION

Calcium (Ca^{2+}) signaling is crucial in the physiology of cells regulating functions as development, muscle contraction, neurotransmission, secretion and even cell death (Berridge, Lipp, & Bootman, 2000; Brini, Cali, Ottolini, & Carafoli, 2014). In fact, cellular processes can be specifically switched on or off depending on cytosolic Ca^{2+} concentration (Bootman & Bultynck, 2020). Different cell types use a plethora of molecules involved in Ca^{2+} signaling in order to control and tightly modulate different cellular functions. In fact, Ca^{2+} dysregulation is involved in the etiology of many disorders, especially in the central nervous system where it has been associated with neurodegenerative diseases, including Alzheimer´s disease (AD), Parkinson´s disease, bipolar disorders, schizophrenia and autism (Bezprozvanny & Mattson, 2008).

Among all cell types in adult brain, microglial cells constitute the first and main line of defense against injury. This requires a cellular activation that implies morphological transformation with changes in gene expression, release of factors into the environment, proliferation, migration and phagocytic activity (Kettenmann, Hanisch, Noda, & Verkhratsky, 2011; Wolf, Boddeke, & Kettenmann, 2017). Although many triggers of microglial activation are known, the underlying subcellular mechanisms are not clear yet. Their description is crucial to understand the presumed dual role found for activated microglia in different neurodegenerative pathologies. Microglia can play a neuroprotective or beneficial role on one hand, but on the other hand they can also contribute to neuroinflammation with detrimental effects (Arcuri, Mecca, Bianchi, Giambanco, & Donato, 2017; Du, Wang, & Geng, 2018; Martin-Estebane & Gomez-Nicola, 2020; Tang & Le, 2016).

Emerging evidence indicates that intracellular Ca^{2+} signaling could play a critical role in the activation of microglia (Brawek & Garaschuk, 2013; Hoffmann, Kann, Ohlemeyer, Hanisch, & Kettenmann, 2003). *In vivo* studies have shown that the variations of cytosolic Ca^{2+} concentration ($[Ca^{2+}]_c$) are minimal in resting microglia, whereas great fluctuations occur during microglial activation (Eichhoff, Brawek, & Garaschuk, 2011; Olmedillas Del Moral, Asavapanumas, Uzcategui, & Garaschuk, 2019; Reddish, Miller, Gorkhali, & Yang, 2017; Tvrdik & Kalani, 2017). Thus, an increase of $[Ca^{2+}]_c$ occurs in the presence of microglial activators such as the bacterial-endotoxin lipopolysaccharide (LPS) (abd-el-Basset & Fedoroff, 1995), extracellular nucleotides released during brain injury and involving P2X/P2Y receptors (James & Butt, 2002; Koizumi et al., 2007; Langfelder, Okonji, Deca, Wei, & Glitsch, 2015; Ohsawa et al., 2007) or even the amyloid β-peptide (Aβ), which is neurotoxic in AD (Alawieyah Syed Mortadza, Sim, Neubrand, & Jiang, 2018; Sarlus & Heneka, 2017), among many others. This triggers the signaling cascades that induce a functional response in activated microglia (Hoffmann et al., 2003). However, while Ca^{2+} influx in the cell is well described, the mechanisms involved in Ca^{2+} clearance remain poorly understood. In this respect, the endoplasmic reticulum (ER) is the major Ca^{2+} store in the cell and can participate as fine modulator of Ca^{2+} dynamics. ER membranes contain the sarco(endo)plasmic reticulum Ca^{2+}-ATPase (SERCA), a P-type ion-motive ATPase that reduces $[Ca^{2+}]_c$ by pumping 2 Ca^{2+} ions into the ER lumen at the expense of hydrolysis of 1 molecule of ATP (reviewed in (J. Chen, Sitsel, Benoy, Sepulveda, & Vangheluwe, 2020). Three SERCA genes have been identified in mammals, each with several splice variants. Of these, SERCA2b is the isoform with the highest expression in brain (Baba-Aissa et al., 1996; Baba-Aissa, Raeymaekers, Wuytack, Dode, & Casteels, 1998; Mata & Sepulveda, 2005; Miller, Verma, Snyder, & Ross, 1991). Although the importance of

the ER in microglial Ca^{2+} signaling has been recognized (Brawek & Garaschuk, 2013), the functional relevance of SERCA for microglia modulation remains unknown. Here, we aimed to explore the expression of SERCA2b in activated microglia and its participation in essential microglial functions, such as migration and phagocytosis.

2. MATERIAL AND METHODS

2.1 Immunohistochemistry in control and AD-human brain samples

Paraffin-embedded tissue of medium frontal gyrus from human cerebral cortex of age-matched controls (Braak stage II) and AD-diagnosed patients (Braak stages V-VI) were obtained from The Netherlands Brain Bank (NBB). Procedures, information, and consent forms of the NBB have been approved by the Medical Ethics Committee of the Vrije Universiteit Amsterdam Medical Centre on April 30, 2009. Microtome sections of 8 μm thickness were permeabilized by immersion in 0.05% (v/v) Triton X-100 in phosphate-buffered saline (PBS-T) for 15 min and endogenous peroxidase activity was quenched with PBS-0.5% (v/v) H_2O_2 for 45 min. After blocking with 0.2% (w/v) gelatin, 0.25% (v/v) Triton X-100 in PBS (PBS-G-T) and 0.1 M lysine for 1 h, sections were incubated overnight at room temperature in a humidified chamber with the following primary antibodies: the monoclonal anti-SERCA2 (clone IID8, Sigma, diluted 1:500 in PBS-G-T), the polyclonal microglial marker Iba1 (1:500, Wako) or the monoclonal anti-Aβ (1:500, STAB VIDA) diluted in PBS-G-T. Sections were subsequently washed in PBS-T and incubated with biotinylated goat anti-mouse or -rabbit antibodies (1:200, Sigma), respectively, and then with ExtrAvidin-peroxidase (1:200, Sigma). The immunodetection was carried out using 0.03% (w/v) 3,3-

diaminobenzidine tetrahydrochloride and 0.2% H_2O_2. Sections were dehydrated and mounted with Eukitt (Panreac) for observation under the microscope. Alternatively, double immunofluorescence was performed with both primary antibodies and the corresponding Alexa594 and Alexa488 secondary antibodies (1:2000, Molecular Probes). For visualization of nuclei, 3 µM 4´,6-diamidino-2-phenylindole (DAPI, Sigma) as a DNA-specific dye was used. Slides were mounted in FluorSave (Calbiochem) and analyzed with a Zeiss Axiophot fluorescence microscope with Axiocam 506 color camera and the ZEN 2.3 Lite Software. Negative controls were performed for every set of experiments by omitting the primary antibodies from the procedure.

2.2 BV2-cell line and microglial primary cultures

BV2 cells were cultured in RPMI medium containing 10% (v/v) fetal bovine serum (GIBCO), supplemented with 2 mM L-glutamine, 100 U/ml penicillin, 100 µg/ml streptomycin and incubated at 37°C in a humidified atmosphere of 5% CO_2.

Primary cultures of mouse brain microglia were prepared as modifications of established procedures (Bolos et al., 2016; Neubrand et al., 2014). Briefly, newborn (1-day old) C57BL/6 mice were obtained from the animal facility service of the Scientific Instrument Centre of the University of Granada (UGR), and experiments were performed with approval of the UGR Ethical Committee. Briefly, meninges-free cerebral cortex were dissected and collected in DMEM with 4.5 g/l D-Glucose, 4 mM glutamine, 10% (v/v) fetal bovine serum), 10% (v/v) horse serum and 100 U/ml penicillin, 100 µg/ml streptomycin (all reagents from GIBCO). After disaggregation and homogenization, cells were seeded and incubated at 37°C with 5% CO_2 for 10-12 days. Then, cultures were softly shaken at 37ºC for 2 h and the primary microglia-enriched

supernatant was subcultured in the same medium for 2 days before experiments. Cultures of microglia showed >90% of microglial marker Iba1-positive cells by immunocytochemistry. Cell activation was induced by 100 ng/ml bacterial lipopolysaccharide (LPS, serotype 0111:B4, Sigma), according to (Henn et al., 2009).

2.3 Immunocytochemistry

BV2 cells or primary microglia (25 000 cells) were seeded onto 12 mm (diameter) round glass coverslips coated with 0.1 mg/ml poly-D-lysine. After treatment, cells were fixed with 4% paraformaldehyde in PBS for 20 min. Then, cells were permeabilized with 0.2% (v/v) Triton X-100 in PBS, and blocked with 3% bovine serum albumin (BSA) in PBS for 1 h. Subcellular co-localization of proteins was determined by incubation with the polyclonal rabbit anti-SERCA2b (1:500, (Wuytack, Eggermont, Raeymaekers, Plessers, & Casteels, 1989), or the monoclonal anti-β tubulin (1:1000, Sigma) primary antibodies diluted in the blocking solution for 1 h. Fluorescence labelling was obtained by the corresponding secondary antibodies Alexa594 goat anti-rabbit and Alexa488 goat anti-mouse (1:2000, Molecular Probes), and DAPI for nuclei staining. Images were taken with the Zeiss Axiophot fluorescent microscope.

2.4 Cell analysis

Images were analyzed by Image J software (version 1.50i, NIH). The cell morphology was characterized by analysis of form factor and aspect ratio of individual cells, according to (Alawieyah Syed Mortadza et al., 2018). The form factor values range between 0 and 1, where values closer to 0 indicate elongated cell shapes and values closer to 1 correspond to a circle. Values of aspect ratio start at 1.0, which indicates a circle, while ascending values indicate enhanced cell ramification and elongation.

Quantification of immunostaining intensities were determined in terms of *Mean Gray Value* (average gray value within the selection) or *Integrated Density* (the product of *Area* and *Mean Gray Value*). The number of mitotic cells was quantified according to an established method (Tarnowski et al., 1993). Briefly, DAPI nuclear staining was used to identify condensed chromosomes of mitotic cells compared to a more uniform ovally shaped nucleus in interphase cells.

2.5 Preparation of protein extracts and Western blotting

Cells were seeded at a density of 1.5 x 10^6 cell per p100 plate or 200 000 cells per well in 6-well plates. After treatments, cells were scraped and pelleted. Protein extracts were prepared using 50 mM Tris/HCl pH 8.0, 0.1 mM EDTA, 0.5 % Triton X-100 and 12.5 mM β-mercaptoethanol as lysis buffer, and vortexing every 5 min for 45 min on ice. After centrifugation at 16 000 x g for 15 min, protein extracts were obtained in the supernantant. The protein concentration was measured by the Bio-Rad Protein Assay using bovine serum albumin as protein standard.

Twenty micrograms of extracts were electrophoresed in 7.5% (w/v) SDS-polyacrylamide gels and transferred to polyvinylidene difluoride (PVDF) membranes using a Trans-Blot SD semidry system (Bio-Rad). After blocking in Tris-buffered saline (TBS) containing 5% (w/v) of non-fat dry milk and 0.3% Tween 20 for 1 h, immunostaining reactions were performed by incubating the membranes for 3 h at room temperature with the following primary antibodies diluted in TBS-1% (v/v) Tween 20: anti-SERCA2b (1:1000), Iba1 (1:500), anti-β actin (1:3000, Sigma), anti-PCNA (1:3000, Sigma) and anti β-tubulin (1:3000). Afterwards, membranes were incubated for 1 h at room temperature with peroxidase-conjugated secondary antibodies (1:5000, Bio-

Rad) and revealed with ECL substrate (Millipore) using the ChemiDoc-It (UVP) and VisionWorks LS software.

2.6 Scratch assay

BV2 or primary microglia were grown in 6-well plates at density of 250 000 cells per well. The monolayer was scratched with a sterile 200-µl pipette tip in a straight line along the diameter of the well and washed three times with sterile PBS. Migration of the cells to the open scratch was recorded using a Leica DM-IRB inverted microscope with a CTI-controller 3700 Digital System at 37°C in a humidified atmosphere of 5% CO_2. BV2 cells were alternatively seeded onto poly-D-lysine-coated glass coverslips at a density of 50 000 cells in 24-well plates, followed by fixation and staining for the actin cytoskeleton with phalloidin-FITC (1:50, Sigma) or immunostaining with anti-Aβ (1:500) and anti β-tubulin (1:1000) antibodies.

2.7 Phagocytosis assays

BV2 or primary microglial cells were seeded at a density of 25 000 cells per coated-glass coverslips. Fluorescent red-latex beads (mean particle diameter 1 µm, Sigma) were pre-opsonized in 50% FBS in sterile PBS for 1 h and loaded to the cells at concentrations of 50 beads per cell for 4 h at 37ºC. After that, remaining beads were washed off the cells twice and cells were fixed in 4% paraformaldehyde in PBS for 15 min at room temperature and mounted in glass slides with FluorSave mounting medium. Alternatively, cells were incubated for 4 h with 100 nM oligomeric 1-42 amyloid β-peptide. For preparation, dry Aβ peptide (Anaspec) was dissolved in alkaline conditions and further incubated at 37ºC for 12 h for oligomerization (Berrocal, Sepulveda, Vazquez-Hernandez, & Mata, 2012). Phagocytized peptides were identified by

immunostaining with anti-Aβ antibody (1:500). Immunostaining with anti β-tubulin (1:500) or the rat monoclonal anti-CD68 (1:500, AbD Serotec), antibodies and nuclear staining with DAPI were used for further analysis. Images were captured with the Zeiss Axiophot fluorescent microscope or with a Leica TCS SP5 confocal microscope to obtain orthogonal projections to verify that observed particles were inside the cells.

2.8 Data processing and statistical analysis

Data were processed and analyzed with the SigmaPlot v10 software (SPSS Inc, Chicago, IL) and significant differences were determined by unpaired Student´s *t*-test. Statistical significance was assumed at $p \leq 0.05$.

3. RESULTS

3.1 SERCA2b is highly expressed in activated microglia from AD-affected brains

Immunohistochemistry was performed with the antibody against the ER Ca^{2+}-ATPase SERCA2b in samples of control and AD-affected human brains (Fig. 1A). We observed the expected SERCA2b staining in the cytoplasm of the soma and dendritic trunk of neurons in both controls and samples affected by AD, according to the known neural ER distribution (Baba-Aissa et al., 1996; Mata & Sepulveda, 2005; Sepulveda, Hidalgo-Sanchez, & Mata, 2004). Additionally, in AD brains the antibody also strongly reacted with small cells, which resembled microglia features, as shown by immunohistochemistry with the well-known microglial marker Ionized calcium-binding adaptor protein-1 (Iba1, Fig. 1B). Iba1 showed a uniform cytosolic distribution, including cell body and branches, allowing a good recognition of microglial

morphology (Ahmed et al., 2007; Imai, Ibata, Ito, Ohsawa, & Kohsaka, 1996; Ito et al., 1998). This revealed two microglial populations each corresponding to a different functional state: ramified cells, characterized by small cell bodies and numerous long branching processes, which were mostly surveillant resident microglia, and cells with very short extensions and amoeboid shape that correspond to activated microglia. The latter showed a similar appearance as cells with high SERCA2b expression observed in the AD samples. Double immunofluorescence confirmed that the Iba1-positive cells with SERCA2b overexpression corresponded to activated microglia (Fig. 1C). Since the SERCA2b staining is mainly found in the cell body according to ER localization, and all Iba1-positive cells showed SERCA2b staining, we used Iba1 for additional analysis of cell morphology parameters in Iba1/SERCA2b-immunopositive cells of control and AD samples (Fig. 1D). We observed a shift from more ramified cells in control brains to more amoeboid cells in AD brains. We also quantified Iba1 levels in microglial cells (Fig. 1E), but no significant differences were observed among cells, even with different morphology, in controls and AD brains. Conversely, the SERCA2b content was 1.4 times higher in microglial cells of AD brains than in controls (Fig. 1F), while the expression of SERCA2b did not appear altered in neurons. In addition, double immunohistochemistry performed in AD samples with the SERCA2b antibody and the Aβ antibody to reveal senile plaques showed high expression of SERCA2b in amoeboid microglial cells in close topographical association with senile plaques (Fig. 1G).

In order to further explore the relevance of SERCA2b in microglial functions, *in vitro* studies were carried out using the microglial BV2 cell line and primary cultures of microglia from mouse brain, as described below.

3.2 The SERCA2b Ca^{2+} pump is upregulated in LPS-activated BV2 cells

We analyzed the expression and localization of SERCA2b in the murine microglial BV2 cell line. Immunocytochemistry showed the expected subcellular localization of SERCA2b in the cell body, where ER is widely extended, but not in cellular processes visualized by β-tubulin immunostaining (Fig. 2A). To promote cell activation *in vitro*, BV2 cells were treated with the bacterial endotoxin LPS. Although it does not promote the typical morphologic transformation from ramified to more round cells in BV2 cells, it induces many other characteristics of activated microglia (abd-el-Basset & Fedoroff, 1995; Henn et al., 2009; Hoffmann et al., 2003). Thus, LPS-activated BV2 cells just showed a slight change in morphology (Fig. 2B), but we observed a significant increase in the integrated density corresponding to the ER-localized SERCA2b (Fig. 2C). Accordingly, the analysis of protein content by Western blots revealed an increase of SERCA2b expression after LPS treatment compared with control BV2 cells (Fig. 2D), while the microglial marker Iba1, that is also a Ca^{2+}-binding protein, did not change its expression level after LPS treatment (Fig. 2E).

3.3 Specific inhibition of SERCA by thapsigargin stimulates BV2 cell migration

Scratch assays were carried out to analyze the migration capacity of BV2 cells and the involvement of SERCA2b. In controls, numerous BV2 cells migrated into the open scar after 6 h, due to the lack of contact inhibitions among cells. Cells formed an interesting and well-ordered row parallel to the scratch boundary (Fig. 3A). As expected, BV2 cell migration was strongly increased by addition of LPS to the assay, although it was less organized. In order to analyze the Ca^{2+} involvement in this process we used thapsigargin, a selective and powerful SERCA inhibitor that blocks the pump to an irreversible state at nM concentrations (Lytton, Westlin, & Hanley, 1991; Sagara, Fernandez-Belda, de Meis, & Inesi, 1992; Sagara & Inesi, 1991). It is well known that

SERCA inhibition produces a passive leak of Ca^{2+} from the ER to the cytosol, inducing an increase in $[Ca^{2+}]_c$ (Thastrup, Cullen, Drobak, Hanley, & Dawson, 1990; Toescu, Moller, Kettenmann, & Verkhratsky, 1998) that may affect cellular migration. Remarkably, after 6 h, the inhibition of SERCA activity by thapsigargin induced a higher increase in BV2 cell migration into the open scar than that observed in LPS-treated cultures (Fig. 3B).

Since we observed that cells in the unscratched region acquired a more rounded shape in the presence of thapsigargin, we checked cell adherence capacities by extensive washing after 6 h-treatment to remove less-adhered cells. As shown in Fig. 3A,B, no differences were found between control and LPS-treated cells before and after washing. However, in the presence of thapsigargin, those cells that had migrated to the scratch kept their adherence properties better than cells from the unscratched region.

We further analyzed migration dynamics with time-lapse experiments in the three conditions of cell culture, i.e. control, LPS-treated and thapsigargin-treated cultures (Supplementary videos VS1-3). As can be seen in Fig. 3C, a clear change in the slope of the curves representing cell areas in the scratch occurred from 3.5 h to 6 h in control and thapsigargin-treated cultures. This change was even more evident in the presence of thapsigargin. Thus, inhibition of SERCA with thapsigargin enhanced cell migration presumably by inducing a maintained high $[Ca^{2+}]_c$.

In order to analyze if changes in protein expression levels of SERCA2b were responsible for the differences found in migration and adherence capacities of cells inside or outside the scratch, we determined the integrated density corresponding to SERCA2b staining in BV2 cells at 0 h and after 6 h in the scratch assay in the absence and presence of thapsigargin (Fig. 3D). As shown, no significant changes in SERCA2b expression were observed. This result points to inhibition on SERCA activity (and not

protein expression changes) and its effect on cytosolic Ca^{2+} dynamics as key factors for the enhanced cell migration.

To determine if cell proliferation occurred in the scratch assays, the number of mitotic cells was quantified by DAPI staining at the end of each assay (Fig. 3E). We found more mitosis outside the scratched area, with no significant differences between control and LPS conditions. Interestingly, the number of mitotic cells was drastically reduced by thapsigargin, and they were found only in the scratched area. We also checked the expression of the proliferation marker PCNA, and found no differences between the experimental conditions (Fig. 3F). In addition, MTT assays were performed to score BV2 cell viability in the three conditions. LPS and the thapsigargin-solvent DMSO did not affect viability, but the cell survival was reduced by 25% after 6 h of treatment with thapsigargin compared with the control (Supplementary Fig. S1).

To further analyze the effect of thapsigargin on microglial migration, we used fluorescent phalloidin staining to visualize the actin cytoskeleton at different time points during the scratch assay (Fig. 3G). At the beginning of the experiment, BV2 cells exhibited thin filopodia, a known cellular mechanism in microglial surveillance for exploring surroundings, but just after 5 min cells extended protrusions toward the scratch, known as lamellipodia, in both control and thapsigargin-treated cultures. This initial polarization is required to set the cell locomotion to a particular direction. However, after 2 h, cells treated with thapsigargin turned to an amoeboid morphology in the scratch, exhibiting strong staining of cortical actin and blebs used for migration, corresponding to less adhered cells that migrate faster, probably using a type of migration called amoeboid motility (Schaks, Giannone, & Rottner, 2019). We also compared phalloidin staining in cells outside the scratch after 6 h (Fig. 3H). As shown. cells in control medium still displayed thin filopodia similar to the 0 h timepoint, while

cells treated with thapsigargin exhibited an amoeboid morphology without filopodia or lamellipodia.

3.4 SERCA2b is also upregulated in activated primary microglia, and its inhibition by thapsigargin stimulates microglial migration

In order to corroborate the results obtained in BV2 cells, we also analyzed SERCA2b expression in microglia from primary cultures prepared from mouse brain. Immunocytochemistry showed the SERCA2b expression in microglial cells with a subcellular localization compatible with its presence in the ER (Fig. 4A), but also the expected change in cell morphology after induction of activation with LPS (Fig. 4A, B). Similar to BV2 cells, LPS-activated microglia showed an increase in the integrated density corresponding to the SERCA2b staining (Fig. 4C). This was correlated with increased levels of SERCA2b protein after LPS-mediated activation, as detected by Western blot (Fig. 4D). We also tested Iba1 expression in these cultures (Fig. 4E). A small increase of Iba1 expression was observed in LPS-activated primary microglia. This observation slightly differs from the results obtained with LPS-activated BV2 cells (Fig. 2E) or microglia of control and AD-brains (Fig 1E), but it is not unexpected considering that some variations in Iba1 expression level between studies and brain regions have been reported (Hopperton, Mohammad, Trepanier, Giuliano, & Bazinet, 2018).

We also analyzed the effect of SERCA inhibition on primary microglia migration in scratch assays (Fig. 5). Cells from primary culture migrated to cover the scratch, although they migrated more slowly comparing with the BV2 cells. After specific inhibition of SERCA by thapsigargin for 48 h, cell migration was increased compared with control and LPS-treated cells (Fig. 5A), similar to the results observed in BV2

cells. Cellular adherence in the scratch was also better preserved after washing in thapsigargin-treated cells. Analysis of migration dynamics in the presence of thapsigargin also showed a change in the slope of the curves, in this case after 24 h, reaching the highest number of cells in the scratch region at the end of the assay (Fig. 5B), as shown above for BV2 cells (Fig. 3B).

3.5 Inhibition of SERCA by thapsigargin decreases phagocytosis in BV2 and primary microglial cells

We analyzed the involvement of the SERCA pump in the phagocytic capacity of BV2 cells and primary microglia by using fluorescent red-latex beads (Fig. 6). Before fixation, cells were extensively washed to remove beads adhering to the cell surface, and the effective internalization of beads into the cells was verified in orthogonal projections of confocal microscopy (Fig. 6A). Then, we quantified cells that did not phagocytose (0), or phagocytosed few (1-4) or many (>5) beads. In the presence of LPS, we detected an increase in the percentage of cells that phagocytosed few (in BV2 cells) and many (in primary microglia) beads as compared to their controls. However, the treatment with thapsigargin led to a significant reduction of the phagocytic capacity in both BV2 and primary microglial cells.

To analyze if SERCA was also involved in receptor-triggered phagocytosis, we determined microglial phagocytic activity after addition of the Aβ peptide, a hallmark in AD. The Aβ peptide is recognized in microglia by Toll-like receptors, such as TLR4, which also recognize LPS, causing Ca^{2+} influx to the cytosol and triggering a signaling cascade that leads to microglial activation (Molteni, Gemma, & Rossetti, 2016; Walter et al., 2007). We specifically used oligomeric $A\beta_{42}$, since an effect of the aggregation state of the peptide on the microglial phagocytic efficiency has been described

(Gouwens, Makoni, Rogers, & Nichols, 2016; Paranjape, Gouwens, Osborn, & Nichols, 2012; Sun, Chen, & Wang, 2015). In these experiments, we also extensively washed the cells before fixation and verified that Aβ was inside the cells by confocal microscopy (Fig. 7A). In both cultures of BV2 cells and primary microglia, control cells showed a considerable phagocytosis of Aβ peptide (Fig. 7), proving the efficiency of these cells in removing toxic Aβ. This was not increased by addition of LPS, which binds to the same receptor. However, similarly to the experiments with latex beads, a significant reduction of Aβ phagocytosis was found in BV2 and primary microglial cells treated with the SERCA inhibitor thapsigargin. These results demonstrated that inhibition of SERCA activity also strongly prevented receptor-induced phagocytosis in microglial cells.

Furthermore, we examined CD68 expression, as a marker for the microglial capacity of phagocytosis (Walker & Lue, 2015; Zotova et al., 2013). Although there was some CD68 expression in resting BV2 cells, cells phagocytosing Aβ significantly increased CD68 expression in comparison with cells in the absence of Aβ or in the presence of both Aβ and thapsigargin (Fig. 8).

Considering that our results point to opposite effects of SERCA inhibition on phagocytosis and migration, we analyzed both processes following the application of Aβ in the scratch assays (Fig. 9). The presence of Aβ induced a significant reduction in the coverage of the scratch in both control and thapsigargin conditions. On the other hand, under control conditions, the most migrating cells found in the middle of the scratch showed a significant reduction in Aβ phagocytosis, while the non- or less-migrating cells closer to the scratch exhibited a slightly higher phagocytosis but not reaching the phagocytic capacity found in cultures without scratch stimulation (Fig. 9D). These results on Aβ phagocytosis support the view that microglia have a low capacity of phagocytosis while they are involved in active migration, and vice versa. In

the presence of thapsigargin, the phagocytosis was impaired in both migrating and non-migrating cells (Fig. 9C-D), as shown before (Figs. 6 and 7).

4. DISCUSSION

This work analyzes the protein expression and subcellular localization of the ER Ca^{2+}-ATPase SERCA2b in microglial cells as well as its contribution to microglial functions. We showed that SERCA2b is highly expressed in activated microglia from AD-brains as well as after activation *in vitro* with LPS in BV2 murine microglial cell line and primary microglia isolated from mouse brain. By exploring a gene expression database for microglia (Friedman et al., 2018), we have found our results at protein expression levels in good agreement with RNA seq data showing a significant higher expression of SERCA2 transcript in microglia extracted from LPS-treated mice (Srinivasan et al., 2016), and in embryonic and perinatal microglia, which are more activated than the branched adult microglia of healthy brains (Matcovitch-Natan et al., 2016). This enhanced SERCA2b expression can be understood as a cellular feedback aimed to restore the maintained high $[Ca^{2+}]_c$ caused by cell activation. Additionally, this upregulation of SERCA2b protein seems to be specific for microglial cells, since changes in its expression were not observed in neurons of AD-affected brain regions in respect to controls either by immunohistochemistry (see Fig. 1) or by Western blot (Berrocal et al., 2015).

In order to study the contribution of SERCA2b to Ca^{2+} signaling in microglia, we used the specific SERCA-inhibitor thapsigargin, which inhibits specifically the pump to an irreversible state (Sagara & Inesi, 1991). In fact, we have used 100 nM thapsigargin in

order to specifically block the SERCA pump, since micromolar concentrations of thapsigargin can inhibit other Ca^{2+} pumps as the SPCA (J. Chen et al., 2017). The SERCA inhibition prevents Ca^{2+} refilling of the ER, producing a net passive leak from the ER store that results in ER emptying and increased $[Ca^{2+}]_c$ (Thastrup et al., 1990). Besides the Ca^{2+} depletion in the ER, the SERCA arrest may also induce a subsequent Ca^{2+} influx from the extracellular medium via store-operated channel entry (SOCE), since microglia express Ca^{2+} release-activated Ca^{2+} (CRAC) channels, similar to other immune cells (Parekh, 2010). In fact, SOCE has been reported for BV2 cells and primary microglia (Bagur & Hajnoczky, 2017; Heo, Lim, Nam, Lee, & Kim, 2015; Michaelis, Nieswandt, Stegner, Eilers, & Kraft, 2015), and the activation of this capacitive Ca^{2+} pathway can sustain long-lasting signals (Toescu et al., 1998). Therefore, the Ca^{2+} depletion in the ER via SERCA inhibition may trigger long-term effects on $[Ca^{2+}]_c$ homeostasis that could explain the change in the slope and the highest stimulation of cell migration showed in our scratch assays in the presence of thapsigargin compared with the LPS-treatment. Combined incubation with LPS and thapsigargin showed less cell migration than each separate compound in both BV2 and primary microglia (data not shown), suggesting a negative effect via cytosolic Ca^{2+} overload from both plasma membrane and ER.

Moreover, the inhibition of SERCA by thapsigargin produced a significant effect on actin cytoskeleton dynamics, changing microglial morphology to an amoeboid shape with blebs and ruffles, in line with faster moving cells. Actin dynamics are critical in cell migration and many actin-binding and -severing proteins are activated by high levels of Ca^{2+} in the cytosol (Choe et al., 2002; Ito et al., 1998). The change in morphology caused by thapsigargin also reduced adhesion in resting cells, but less in migrating cells, maybe because the formation of focal contacts required for moving

forward serves as anchorage sites. On the other hand, microglial activation may lead to readjusting mechanisms for Ca^{2+} handling despite Ca^{2+} depletion in the ER in migrating cells. This is worthy to investigate further, as compensation of different Ca^{2+} stores have been seen in other experimental models (Sepulveda, Vanoevelen, Raeymaekers, Mata, & Wuytack, 2009).

Since microglia are the primary phagocytes in the brain parenchyma, they are responsible for clearance of apoptotic or necrotic cells (Green, Oguin, & Martinez, 2016) and for the removal of pathogens (Nau, Ribes, Djukic, & Eiffert, 2014), neurotoxic peptides and protein aggregates (Hansen, Hanson, & Sheng, 2018; Hoffmann et al., 2016). Hence, microglia play a central protective role in neurodegeneration. However, excessive pruning of synapses (Z. Chen et al., 2014; Rajendran & Paolicelli, 2018; Sierra, Abiega, Shahraz, & Neumann, 2013) or even phagoptosis of neurons (Brown & Neher, 2012, 2014) by microglia can also be enhanced in pathological conditions, reflecting the still unraveled dual role of microglia in neurodegenerative diseases, e.g. defective or overactivated phagocytosis has been found in AD and other neurodegenerative diseases (Janda, Boi, & Carta, 2018; Krasemann et al., 2017; Neniskyte, Neher, & Brown, 2011). Here, we showed the critical importance of Ca^{2+} transport into the ER on the modulation of phagocytic activity, since SERCA inhibition led to impaired phagocytosis. In addition, this impairment could be due to the effect of thapsigargin on cell morphology, as we observed a reduction of filopodia involved in microglial surveillance.

Our treatment during 4-6 h with 100 nM thapsigargin induced a change in morphology from branched to amoeboid cells but it did not drastically affect cell viability, as observed in the MTT assay. In fact, we did not visualize symptoms of cell damage by microscopy, such as cell blebbing (by phase-contrast), pyknosis or nuclear

fragmentation (by DAPI staining) or disruption of cytoskeletal elements (by actin and tubulin stainings). However, it has been reported that prolonged exposure to thapsigargin can cause stress in the ER and other Ca^{2+} stores, and subsequently may evoke the unfolded protein response, caspase activation, mitochondrial release of apoptotic factors and activation of Ca^{2+}-dependent endonucleases, eventually resulting in cell death (Foufelle & Fromenty, 2016; Tabas & Ron, 2011). In fact, local SERCA2b inhibition by thapsigargin-derivates and its effect on Ca^{2+} signaling has been recently explored as a potential anti-cancer therapy (Akinboye, Brennen, Denmeade, & Isaacs, 2019; Doan et al., 2015; Mahalingam et al., 2016). Although SERCA2b is ubiquitously expressed, this strategy relies on local activation of an inactive thapsigargin prodrug in the tumor environment, which may cause death specifically in the cancer cells.

One of the most remarkable results of our study was the opposite effect caused by SERCA inhibition on microglial migration and phagocytosis. Many cellular processes can be specifically switched on or off depending on $[Ca^{2+}]_c$ (Bootman & Bultynck, 2020), and our result suggests an opposite effect of $[Ca^{2+}]_c$ on the molecular mechanisms regulating both processes. Thus, different activation states may be obtained depending on the type or strength of the extracellular signal. In fact, different extracellular nucleotides released after brain injury regulate different functions of activated microglia. Extracellular ATP stimulates chemotactic microglial migration (Haynes et al., 2006), whereas UDP promotes microglial phagocytosis (Inoue, 2007; Koizumi et al., 2007). In addition, high or low ATP concentrations induce oscillations in $[Ca^{2+}]_c$ after activation of P2X7 or P2X4 receptors, respectively (Gilbert et al., 2016). Therefore, the same nucleotide can induce variable changes in Ca^{2+} dynamics in a concentration-dependent manner. These changes could promote, in turn, a shift from the migratory to the phagocytic state. It seems reasonable that after a first signal of brain

injury, microglial cells need to migrate but not phagocyte, and once that they are in the damaged area, microglia begin phagocytic activity for clearance of dying neurons or other toxic substances (Jonas et al., 2012). Accordingly, it has been reported in photodegenerative experiments that microglial cells migrate crossing all retinal layers until they reach the outer nuclear layer where they exhibit phagocytic activity of degenerating photoreceptors (Santos et al., 2010). In a similar way, during embryonic development, microglial cells actively migrating to colonize the retina do not phagocytose dead cell debris, which are engulfed by Müller cells (Marin-Teva, Cuadros, Calvente, Almendros, & Navascues, 1999). These *in vivo* observations are consistent with our present *in vitro* results, supporting the view that microglia have a low capacity of phagocytosis while they are involved in active migration. It is tempting to hypothesize that factors triggering activation of microglia are initially in concentrations that favor their migration, and are subsequently decreased to levels that promote phagocytosis. These different concentrations would differentially regulate microglial $[Ca^{2+}]_c$ with the active participation of SERCA2b to alternatively promote molecular pathways responsible for migration or phagocytosis. In this sense, it has been recently reported that BV2 microglia silenced for Iba1, which binds Ca^{2+} and acts as actin-cross linking protein (Sasaki, Ohsawa, Kanazawa, Kohsaka, & Imai, 2001), migrated less, but exhibited increased phagocytic activity (Gheorghe et al., 2020), supporting the important role of Ca^{2+} signaling and cytoskeleton dynamics in these microglial functions.

Recently a new ‘extremely active’ microglial phenotype has been described in pathological states such as AD, known as ‘dark microglia’ (Bisht et al., 2016). Among their ultrastructural characteristics, an extensive and dilated ER stands out. Since Ca^{2+} overload in the ER cause dilatation of cisternae, it is tempting to speculate that this

feature may correlate with the upregulation of SERCA2b we detected *in vitro* as well as in AD-affected brain´s microglia. Moreover, dark microglia present extreme phagocytic activity at the synapse (Bisht et al., 2016), where the modulation of SERCA activity could have a significant impact, opening a window to new therapeutic strategies.

ACKNOWLEDGEMENTS

We are grateful to Prof F. Wuytack (Katholieke Universiteit Leuven, Belgium) for critically reading of the manuscript and kind support, to Prof J. Ávila and Dr M. Bolós (Centre for Molecular Biology Severo Ochoa, CSIC-UAM, Spain) for helpful advice with the primary cultures of microglia, and to Prof. A. Osuna (Dept. of Parasitology, UGR) for his kind gift of phalloidin-FITC. This work was financially supported by grants mP_BS_35-2014 from CEI BioTic Granada, PP2016-PJI05 from University of Granada and A1-CTS-324-UGR18 from FEDER-Junta de Andalucía, Spain (to M.R.S.). We also acknowledge PP2016-PIP08 (to J.N.) from University of Granada, BFU2017-85723-P (to A.M.M.) from Spanish Ministry of Economy and Competitiveness co-financed with FEDER, and G044212N from Flanders Research Foundation (to P.V.). J.M.M.R. received a postgraduate scholarship provided by Ministry of Education, Culture and Sports, Spain.

REFERENCES

abd-el-Basset, E., & Fedoroff, S. (1995). Effect of bacterial wall lipopolysaccharide (LPS) on morphology, motility, and cytoskeletal organization of microglia in cultures. *J Neurosci Res, 41*(2), 222-237. doi:10.1002/jnr.490410210

Ahmed, Z., Shaw, G., Sharma, V. P., Yang, C., McGowan, E., & Dickson, D. W. (2007). Actin-binding proteins coronin-1a and IBA-1 are effective microglial markers for immunohistochemistry. *J Histochem Cytochem, 55*(7), 687-700. doi:10.1369/jhc.6A7156.2007

Akinboye, E. S., Brennen, W. N., Denmeade, S. R., & Isaacs, J. T. (2019). Albumin-linked prostate-specific antigen-activated thapsigargin- and niclosamide-based molecular grenades targeting the microenvironment in metastatic castration-resistant prostate cancer. *Asian J Urol, 6*(1), 99-108. doi:10.1016/j.ajur.2018.11.004

Alawieyah Syed Mortadza, S., Sim, J. A., Neubrand, V. E., & Jiang, L. H. (2018). A critical role of TRPM2 channel in Abeta42 -induced microglial activation and generation of tumor necrosis factor-alpha. *Glia, 66*(3), 562-575. doi:10.1002/glia.23265

Arcuri, C., Mecca, C., Bianchi, R., Giambanco, I., & Donato, R. (2017). The Pathophysiological Role of Microglia in Dynamic Surveillance, Phagocytosis and Structural Remodeling of the Developing CNS. *Front Mol Neurosci, 10*, 191. doi:10.3389/fnmol.2017.00191

Baba-Aissa, F., Raeymaekers, L., Wuytack, F., De Greef, C., Missiaen, L., & Casteels, R. (1996). Distribution of the organellar Ca2+ transport ATPase SERCA2 isoforms in the cat brain. *Brain Res, 743*(1-2), 141-153. doi:10.1016/s0006-8993(96)01037-2

Baba-Aissa, F., Raeymaekers, L., Wuytack, F., Dode, L., & Casteels, R. (1998). Distribution and isoform diversity of the organellar Ca2+ pumps in the brain. *Mol Chem Neuropathol, 33*(3), 199-208.

Bagur, R., & Hajnoczky, G. (2017). Intracellular Ca(2+) Sensing: Its Role in Calcium Homeostasis and Signaling. *Mol Cell, 66*(6), 780-788. doi:10.1016/j.molcel.2017.05.028

Berridge, M. J., Lipp, P., & Bootman, M. D. (2000). The versatility and universality of calcium signalling. *Nat Rev Mol Cell Biol, 1*(1), 11-21. doi:10.1038/35036035

Berrocal, M., Corbacho, I., Vazquez-Hernandez, M., Avila, J., Sepulveda, M. R., & Mata, A. M. (2015). Inhibition of PMCA activity by tau as a function of aging and Alzheimer's neuropathology. *Biochim Biophys Acta, 1852*(7), 1465-1476. doi:10.1016/j.bbadis.2015.04.007

Berrocal, M., Sepulveda, M. R., Vazquez-Hernandez, M., & Mata, A. M. (2012). Calmodulin antagonizes amyloid-beta peptides-mediated inhibition of brain plasma membrane Ca(2+)-ATPase. *Biochim Biophys Acta, 1822*(6), 961-969. doi:10.1016/j.bbadis.2012.02.013

Bezprozvanny, I., & Mattson, M. P. (2008). Neuronal calcium mishandling and the pathogenesis of Alzheimer's disease. *Trends Neurosci, 31*(9), 454-463. doi:10.1016/j.tins.2008.06.005

Bisht, K., Sharma, K. P., Lecours, C., Sanchez, M. G., El Hajj, H., Milior, G., . . . Tremblay, M. E. (2016). Dark microglia: A new phenotype predominantly associated with pathological states. *Glia, 64*(5), 826-839. doi:10.1002/glia.22966

Bolos, M., Llorens-Martin, M., Jurado-Arjona, J., Hernandez, F., Rabano, A., & Avila, J. (2016). Direct Evidence of Internalization of Tau by Microglia In Vitro and In Vivo. *J Alzheimers Dis, 50*(1), 77-87. doi:10.3233/JAD-150704

Bootman, M. D., & Bultynck, G. (2020). Fundamentals of Cellular Calcium Signaling: A Primer. *Cold Spring Harb Perspect Biol, 12*(1). doi:10.1101/cshperspect.a038802

Brawek, B., & Garaschuk, O. (2013). Microglial calcium signaling in the adult, aged and diseased brain. *Cell Calcium, 53*(3), 159-169. doi:10.1016/j.ceca.2012.12.003

Brini, M., Cali, T., Ottolini, D., & Carafoli, E. (2014). Neuronal calcium signaling: function and dysfunction. *Cell Mol Life Sci, 71*(15), 2787-2814. doi:10.1007/s00018-013-1550-7

Brown, G. C., & Neher, J. J. (2012). Eaten alive! Cell death by primary phagocytosis: 'phagoptosis'. *Trends Biochem Sci, 37*(8), 325-332. doi:10.1016/j.tibs.2012.05.002

Brown, G. C., & Neher, J. J. (2014). Microglial phagocytosis of live neurons. *Nat Rev Neurosci, 15*(4), 209-216. doi:10.1038/nrn3710

Chen, J., De Raeymaecker, J., Hovgaard, J. B., Smaardijk, S., Vandecaetsbeek, I., Wuytack, F., . . . Vangheluwe, P. (2017). Structure/activity relationship of thapsigargin inhibition on the purified Golgi/secretory pathway Ca(2+)/Mn(2+)-transport ATPase (SPCA1a). *J Biol Chem, 292*(17), 6938-6951. doi:10.1074/jbc.M117.778431

Chen, J., Sitsel, A., Benoy, V., Sepulveda, M. R., & Vangheluwe, P. (2020). Primary Active Ca(2+) Transport Systems in Health and Disease. *Cold Spring Harb Perspect Biol, 12*(2). doi:10.1101/cshperspect.a035113

Chen, Z., Jalabi, W., Hu, W., Park, H. J., Gale, J. T., Kidd, G. J., . . . Trapp, B. D. (2014). Microglial displacement of inhibitory synapses provides neuroprotection in the adult brain. *Nat Commun, 5*, 4486. doi:10.1038/ncomms5486

Choe, H., Burtnick, L. D., Mejillano, M., Yin, H. L., Robinson, R. C., & Choe, S. (2002). The calcium activation of gelsolin: insights from the 3A structure of the G4-G6/actin complex. *J Mol Biol, 324*(4), 691-702. doi:10.1016/s0022-2836(02)01131-2

Doan, N. T., Paulsen, E. S., Sehgal, P., Moller, J. V., Nissen, P., Denmeade, S. R., . . . Christensen, S. B. (2015). Targeting thapsigargin towards tumors. *Steroids, 97*, 2-7. doi:10.1016/j.steroids.2014.07.009

Du, X., Wang, X., & Geng, M. (2018). Alzheimer's disease hypothesis and related therapies. *Transl Neurodegener, 7*, 2. doi:10.1186/s40035-018-0107-y

Eichhoff, G., Brawek, B., & Garaschuk, O. (2011). Microglial calcium signal acts as a rapid sensor of single neuron damage in vivo. *Biochim Biophys Acta, 1813*(5), 1014-1024. doi:10.1016/j.bbamcr.2010.10.018

Foufelle, F., & Fromenty, B. (2016). Role of endoplasmic reticulum stress in drug-induced toxicity. *Pharmacol Res Perspect, 4*(1), e00211. doi:10.1002/prp2.211

Friedman, B. A., Srinivasan, K., Ayalon, G., Meilandt, W. J., Lin, H., Huntley, M. A., . . . Hansen, D. V. (2018). Diverse Brain Myeloid Expression Profiles Reveal Distinct Microglial Activation States and Aspects of Alzheimer's Disease Not Evident in Mouse Models. *Cell Rep, 22*(3), 832-847. doi:10.1016/j.celrep.2017.12.066

Gheorghe, R. O., Deftu, A., Filippi, A., Grosu, A., Bica-Popi, M., Chiritoiu, M., . . . Ristoiu, V. (2020). Silencing the Cytoskeleton Protein Iba1 (Ionized Calcium Binding Adapter Protein 1) Interferes with BV2 Microglia Functioning. *Cell Mol Neurobiol, 40*(6), 1011-1027. doi:10.1007/s10571-020-00790-w

Gilbert, D. F., Stebbing, M. J., Kuenzel, K., Murphy, R. M., Zacharewicz, E., Buttgereit, A., . . . Friedrich, O. (2016). Store-Operated Ca(2+) Entry (SOCE)

and Purinergic Receptor-Mediated Ca(2+) Homeostasis in Murine bv2 Microglia Cells: Early Cellular Responses to ATP-Mediated Microglia Activation. *Front Mol Neurosci, 9*, 111. doi:10.3389/fnmol.2016.00111

Gouwens, L. K., Makoni, N. J., Rogers, V. A., & Nichols, M. R. (2016). Amyloid-beta42 protofibrils are internalized by microglia more extensively than monomers. *Brain Res, 1648*(Pt A), 485-495. doi:10.1016/j.brainres.2016.08.016

Green, D. R., Oguin, T. H., & Martinez, J. (2016). The clearance of dying cells: table for two. *Cell Death Differ, 23*(6), 915-926. doi:10.1038/cdd.2015.172

Hansen, D. V., Hanson, J. E., & Sheng, M. (2018). Microglia in Alzheimer's disease. *J Cell Biol, 217*(2), 459-472. doi:10.1083/jcb.201709069

Haynes, S. E., Hollopeter, G., Yang, G., Kurpius, D., Dailey, M. E., Gan, W. B., & Julius, D. (2006). The P2Y12 receptor regulates microglial activation by extracellular nucleotides. *Nat Neurosci, 9*(12), 1512-1519. doi:10.1038/nn1805

Henn, A., Lund, S., Hedtjarn, M., Schrattenholz, A., Porzgen, P., & Leist, M. (2009). The suitability of BV2 cells as alternative model system for primary microglia cultures or for animal experiments examining brain inflammation. *ALTEX, 26*(2), 83-94.

Heo, D. K., Lim, H. M., Nam, J. H., Lee, M. G., & Kim, J. Y. (2015). Regulation of phagocytosis and cytokine secretion by store-operated calcium entry in primary isolated murine microglia. *Cell Signal, 27*(1), 177-186. doi:10.1016/j.cellsig.2014.11.003

Hoffmann, A., Ettle, B., Bruno, A., Kulinich, A., Hoffmann, A. C., von Wittgenstein, J., . . . Schlachetzki, J. C. M. (2016). Alpha-synuclein activates BV2 microglia dependent on its aggregation state. *Biochem Biophys Res Commun, 479*(4), 881-886. doi:10.1016/j.bbrc.2016.09.109

Hoffmann, A., Kann, O., Ohlemeyer, C., Hanisch, U. K., & Kettenmann, H. (2003). Elevation of basal intracellular calcium as a central element in the activation of brain macrophages (microglia): suppression of receptor-evoked calcium signaling and control of release function. *J Neurosci, 23*(11), 4410-4419.

Hopperton, K. E., Mohammad, D., Trepanier, M. O., Giuliano, V., & Bazinet, R. P. (2018). Markers of microglia in post-mortem brain samples from patients with Alzheimer's disease: a systematic review. *Mol Psychiatry, 23*(2), 177-198. doi:10.1038/mp.2017.246

Imai, Y., Ibata, I., Ito, D., Ohsawa, K., & Kohsaka, S. (1996). A novel gene iba1 in the major histocompatibility complex class III region encoding an EF hand protein expressed in a monocytic lineage. *Biochem Biophys Res Commun, 224*(3), 855-862. doi:10.1006/bbrc.1996.1112

Inoue, K. (2007). UDP facilitates microglial phagocytosis through P2Y6 receptors. *Cell Adh Migr, 1*(3), 131-132. doi:10.4161/cam.1.3.4937

Ito, D., Imai, Y., Ohsawa, K., Nakajima, K., Fukuuchi, Y., & Kohsaka, S. (1998). Microglia-specific localisation of a novel calcium binding protein, Iba1. *Brain Res Mol Brain Res, 57*(1), 1-9. doi:10.1016/s0169-328x(98)00040-0

James, G., & Butt, A. M. (2002). P2Y and P2X purinoceptor mediated Ca2+ signalling in glial cell pathology in the central nervous system. *Eur J Pharmacol, 447*(2-3), 247-260. doi:10.1016/s0014-2999(02)01756-9

Janda, E., Boi, L., & Carta, A. R. (2018). Microglial Phagocytosis and Its Regulation: A Therapeutic Target in Parkinson's Disease? *Front Mol Neurosci, 11*, 144. doi:10.3389/fnmol.2018.00144

Jonas, R. A., Yuan, T. F., Liang, Y. X., Jonas, J. B., Tay, D. K., & Ellis-Behnke, R. G. (2012). The spider effect: morphological and orienting classification of

microglia in response to stimuli in vivo. *PLoS One, 7*(2), e30763. doi:10.1371/journal.pone.0030763

Kettenmann, H., Hanisch, U. K., Noda, M., & Verkhratsky, A. (2011). Physiology of microglia. *Physiol Rev, 91*(2), 461-553. doi:10.1152/physrev.00011.2010

Koizumi, S., Shigemoto-Mogami, Y., Nasu-Tada, K., Shinozaki, Y., Ohsawa, K., Tsuda, M., . . . Inoue, K. (2007). UDP acting at P2Y6 receptors is a mediator of microglial phagocytosis. *Nature, 446*(7139), 1091-1095. doi:10.1038/nature05704

Krasemann, S., Madore, C., Cialic, R., Baufeld, C., Calcagno, N., El Fatimy, R., . . . Butovsky, O. (2017). The TREM2-APOE Pathway Drives the Transcriptional Phenotype of Dysfunctional Microglia in Neurodegenerative Diseases. *Immunity, 47*(3), 566-581 e569. doi:10.1016/j.immuni.2017.08.008

Langfelder, A., Okonji, E., Deca, D., Wei, W. C., & Glitsch, M. D. (2015). Extracellular acidosis impairs P2Y receptor-mediated Ca(2+) signalling and migration of microglia. *Cell Calcium, 57*(4), 247-256. doi:10.1016/j.ceca.2015.01.004

Lytton, J., Westlin, M., & Hanley, M. R. (1991). Thapsigargin inhibits the sarcoplasmic or endoplasmic reticulum Ca-ATPase family of calcium pumps. *J Biol Chem, 266*(26), 17067-17071.

Mahalingam, D., Wilding, G., Denmeade, S., Sarantopoulas, J., Cosgrove, D., Cetnar, J., . . . Carducci, M. (2016). Mipsagargin, a novel thapsigargin-based PSMA-activated prodrug: results of a first-in-man phase I clinical trial in patients with refractory, advanced or metastatic solid tumours. *Br J Cancer, 114*(9), 986-994. doi:10.1038/bjc.2016.72

Marin-Teva, J. L., Cuadros, M. A., Calvente, R., Almendros, A., & Navascues, J. (1999). Naturally occurring cell death and migration of microglial precursors in the quail retina during normal development. *J Comp Neurol, 412*(2), 255-275.

Martin-Estebane, M., & Gomez-Nicola, D. (2020). Targeting Microglial Population Dynamics in Alzheimer's Disease: Are We Ready for a Potential Impact on Immune Function? *Front Cell Neurosci, 14*, 149. doi:10.3389/fncel.2020.00149

Mata, A. M., & Sepulveda, M. R. (2005). Calcium pumps in the central nervous system. *Brain Res Brain Res Rev, 49*(2), 398-405. doi:10.1016/j.brainresrev.2004.11.004

Matcovitch-Natan, O., Winter, D. R., Giladi, A., Vargas Aguilar, S., Spinrad, A., Sarrazin, S., . . . Amit, I. (2016). Microglia development follows a stepwise program to regulate brain homeostasis. *Science, 353*(6301), aad8670. doi:10.1126/science.aad8670

Michaelis, M., Nieswandt, B., Stegner, D., Eilers, J., & Kraft, R. (2015). STIM1, STIM2, and Orai1 regulate store-operated calcium entry and purinergic activation of microglia. *Glia, 63*(4), 652-663. doi:10.1002/glia.22775

Miller, K. K., Verma, A., Snyder, S. H., & Ross, C. A. (1991). Localization of an endoplasmic reticulum calcium ATPase mRNA in rat brain by in situ hybridization. *Neuroscience, 43*(1), 1-9. doi:10.1016/0306-4522(91)90410-p

Molteni, M., Gemma, S., & Rossetti, C. (2016). The Role of Toll-Like Receptor 4 in Infectious and Noninfectious Inflammation. *Mediators Inflamm, 2016*, 6978936. doi:10.1155/2016/6978936

Nau, R., Ribes, S., Djukic, M., & Eiffert, H. (2014). Strategies to increase the activity of microglia as efficient protectors of the brain against infections. *Front Cell Neurosci, 8*, 138. doi:10.3389/fncel.2014.00138

Neniskyte, U., Neher, J. J., & Brown, G. C. (2011). Neuronal death induced by nanomolar amyloid beta is mediated by primary phagocytosis of neurons by microglia. *J Biol Chem, 286*(46), 39904-39913. doi:10.1074/jbc.M111.267583

Neubrand, V. E., Pedreno, M., Caro, M., Forte-Lago, I., Delgado, M., & Gonzalez-Rey, E. (2014). Mesenchymal stem cells induce the ramification of microglia via the small RhoGTPases Cdc42 and Rac1. *Glia, 62*(12), 1932-1942. doi:10.1002/glia.22714

Ohsawa, K., Irino, Y., Nakamura, Y., Akazawa, C., Inoue, K., & Kohsaka, S. (2007). Involvement of P2X4 and P2Y12 receptors in ATP-induced microglial chemotaxis. *Glia, 55*(6), 604-616. doi:10.1002/glia.20489

Olmedillas Del Moral, M., Asavapanumas, N., Uzcategui, N. L., & Garaschuk, O. (2019). Healthy Brain Aging Modifies Microglial Calcium Signaling In Vivo. *Int J Mol Sci, 20*(3). doi:10.3390/ijms20030589

Paranjape, G. S., Gouwens, L. K., Osborn, D. C., & Nichols, M. R. (2012). Isolated amyloid-beta(1-42) protofibrils, but not isolated fibrils, are robust stimulators of microglia. *ACS Chem Neurosci, 3*(4), 302-311. doi:10.1021/cn2001238

Parekh, A. B. (2010). Store-operated CRAC channels: function in health and disease. *Nat Rev Drug Discov, 9*(5), 399-410. doi:10.1038/nrd3136

Rajendran, L., & Paolicelli, R. C. (2018). Microglia-Mediated Synapse Loss in Alzheimer's Disease. *J Neurosci, 38*(12), 2911-2919. doi:10.1523/JNEUROSCI.1136-17.2017

Reddish, F. N., Miller, C. L., Gorkhali, R., & Yang, J. J. (2017). Calcium Dynamics Mediated by the Endoplasmic/Sarcoplasmic Reticulum and Related Diseases. *Int J Mol Sci, 18*(5). doi:10.3390/ijms18051024

Sagara, Y., Fernandez-Belda, F., de Meis, L., & Inesi, G. (1992). Characterization of the inhibition of intracellular Ca2+ transport ATPases by thapsigargin. *J Biol Chem, 267*(18), 12606-12613.

Sagara, Y., & Inesi, G. (1991). Inhibition of the sarcoplasmic reticulum Ca2+ transport ATPase by thapsigargin at subnanomolar concentrations. *J Biol Chem, 266*(21), 13503-13506.

Santos, A. M., Martin-Oliva, D., Ferrer-Martin, R. M., Tassi, M., Calvente, R., Sierra, A., . . . Cuadros, M. A. (2010). Microglial response to light-induced photoreceptor degeneration in the mouse retina. *J Comp Neurol, 518*(4), 477-492. doi:10.1002/cne.22227

Sarlus, H., & Heneka, M. T. (2017). Microglia in Alzheimer's disease. *J Clin Invest, 127*(9), 3240-3249. doi:10.1172/JCI90606

Sasaki, Y., Ohsawa, K., Kanazawa, H., Kohsaka, S., & Imai, Y. (2001). Iba1 is an actin-cross-linking protein in macrophages/microglia. *Biochem Biophys Res Commun, 286*(2), 292-297. doi:10.1006/bbrc.2001.5388

Schaks, M., Giannone, G., & Rottner, K. (2019). Actin dynamics in cell migration. *Essays Biochem, 63*(5), 483-495. doi:10.1042/EBC20190015

Sepulveda, M. R., Hidalgo-Sanchez, M., & Mata, A. M. (2004). Localization of endoplasmic reticulum and plasma membrane Ca2+-ATPases in subcellular fractions and sections of pig cerebellum. *Eur J Neurosci, 19*(3), 542-551. doi:10.1111/j.0953-816x.2003.03156.x

Sepulveda, M. R., Vanoevelen, J., Raeymaekers, L., Mata, A. M., & Wuytack, F. (2009). Silencing the SPCA1 (secretory pathway Ca2+-ATPase isoform 1) impairs Ca2+ homeostasis in the Golgi and disturbs neural polarity. *J Neurosci, 29*(39), 12174-12182. doi:10.1523/JNEUROSCI.2014-09.2009

Sierra, A., Abiega, O., Shahraz, A., & Neumann, H. (2013). Janus-faced microglia: beneficial and detrimental consequences of microglial phagocytosis. *Front Cell Neurosci, 7*, 6. doi:10.3389/fncel.2013.00006

Srinivasan, K., Friedman, B. A., Larson, J. L., Lauffer, B. E., Goldstein, L. D., Appling, L. L., . . . Hansen, D. V. (2016). Untangling the brain's neuroinflammatory and neurodegenerative transcriptional responses. *Nat Commun, 7*, 11295. doi:10.1038/ncomms11295

Sun, X., Chen, W. D., & Wang, Y. D. (2015). beta-Amyloid: the key peptide in the pathogenesis of Alzheimer's disease. *Front Pharmacol, 6*, 221. doi:10.3389/fphar.2015.00221

Tabas, I., & Ron, D. (2011). Integrating the mechanisms of apoptosis induced by endoplasmic reticulum stress. *Nat Cell Biol, 13*(3), 184-190. doi:10.1038/ncb0311-184

Tang, Y., & Le, W. (2016). Differential Roles of M1 and M2 Microglia in Neurodegenerative Diseases. *Mol Neurobiol, 53*(2), 1181-1194. doi:10.1007/s12035-014-9070-5

Tarnowski, B. I., Sens, D. A., Nicholson, J. H., Hazen-Martin, D. J., Garvin, A. J., & Sens, M. A. (1993). Automatic quantitation of cell growth and determination of mitotic index using DAPI nuclear staining. *Pediatr Pathol, 13*(2), 249-265. doi:10.3109/15513819309048211

Thastrup, O., Cullen, P. J., Drobak, B. K., Hanley, M. R., & Dawson, A. P. (1990). Thapsigargin, a tumor promoter, discharges intracellular Ca2+ stores by specific inhibition of the endoplasmic reticulum Ca2(+)-ATPase. *Proc Natl Acad Sci U S A, 87*(7), 2466-2470. doi:10.1073/pnas.87.7.2466

Toescu, E. C., Moller, T., Kettenmann, H., & Verkhratsky, A. (1998). Long-term activation of capacitative Ca2+ entry in mouse microglial cells. *Neuroscience, 86*(3), 925-935. doi:10.1016/s0306-4522(98)00123-7

Tvrdik, P., & Kalani, M. Y. S. (2017). In Vivo Imaging of Microglial Calcium Signaling in Brain Inflammation and Injury. *Int J Mol Sci, 18*(11). doi:10.3390/ijms18112366

Walker, D. G., & Lue, L. F. (2015). Immune phenotypes of microglia in human neurodegenerative disease: challenges to detecting microglial polarization in human brains. *Alzheimers Res Ther, 7*(1), 56. doi:10.1186/s13195-015-0139-9

Walter, S., Letiembre, M., Liu, Y., Heine, H., Penke, B., Hao, W., . . . Fassbender, K. (2007). Role of the toll-like receptor 4 in neuroinflammation in Alzheimer's disease. *Cell Physiol Biochem, 20*(6), 947-956. doi:10.1159/000110455

Wolf, S. A., Boddeke, H. W., & Kettenmann, H. (2017). Microglia in Physiology and Disease. *Annu Rev Physiol, 79*, 619-643. doi:10.1146/annurev-physiol-022516-034406

Wuytack, F., Eggermont, J. A., Raeymaekers, L., Plessers, L., & Casteels, R. (1989). Antibodies against the non-muscle isoform of the endoplasmic reticulum Ca2(+)-transport ATPase. *Biochem J, 264*(3), 765-769. doi:10.1042/bj2640765

Zotova, E., Bharambe, V., Cheaveau, M., Morgan, W., Holmes, C., Harris, S., . . . Boche, D. (2013). Inflammatory components in human Alzheimer's disease and after active amyloid-beta42 immunization. *Brain, 136*(Pt 9), 2677-2696. doi:10.1093/brain/awt210

[dataset] Morales-Ropero et al. 2020. SERCA2b in microglial functions. The data that support the findings of this study are available from the corresponding author upon reasonable request.

FIGURE LEGENDS

Fig. 1 SERCA2b is highly expressed in activated microglia from Alzheimer´s disease affected brain. A. Immunohistochemistry with the anti-SERCA2b antibody in control (Ctr) and Alzheimer´s disease (AD)-affected medial frontal gyrus from human brain, showing the typical localization of SERCA2b in the ER in neurons (arrows and upper boxes) and highly immunostained small cells in AD-affected brain (arrowheads and lower box). B. Immunohistochemistry with the microglial marker Iba1, revealing ramified, non-activated resident microglia (arrows) in a control brain (left) and microglial cells with very short extensions and amoeboid shape corresponding to activated microglia (arrowheads) in an AD-affected brain. C. Double immunofluorescence with Iba1 (red) and the SERCA2b (green) antibodies, showing low SERCA2b staining in Iba1-positive branched microglia of control brain. High SERCA2b expression and co-localization with Iba1 is found in poorly branched-amoeboid microglia of AD-affected brain. Cell nuclei were stained with DAPI (blue). D. Scatter plot including the morphological parameters form factor and aspect ratio of Iba1/SERCA2b-immunopositive cells in control and AD brains, showing a shift to a higher number of amoeboid cells in AD. E. Integrated density of Iba1 immunostaining in control and AD-affected brains. Ramified cells (r) were considered when the form factor was <0.5 and amoeboid (a) when was >0.5. F. SERCA2b expression in neurons (N) and microglia (M) in control and AD samples. Mean gray value was chosen in order to compare these two cell types because of their different cell body sizes. G. Double immunohistochemistry showing amyloid plaques stained with the amyloid-β antibody and SERCA2b-positive microglial cells (arrows) in AD. Scale bars: 50 μm (A, B, G), 20 μm (C).

Fig. 2 SERCA2b is upregulated in LPS-activated BV2 cells. A. Double immunofluorescence of SERCA2b (red) and β tubulin (green) in BV2 cells cultured in control medium (Ctr) and 100 ng/ml LPS-containing (LPS) medium. Cell nuclei were visualized with DAPI (blue). B. Scatter plot showing the distribution of form factor and aspect ratio parameters of control and LPS-activated BV2 cells. C. Integrated density of SERCA2b immunostaining in controls and LPS-activated cells showing a significantly higher value in the latter condition ($p<0.005$, asterisk). D and E. Representative Western blots using the anti-SERCA2b (D) and the microglial marker Iba1 (E) antibodies. Protein extracts of adult mouse brain (Brain) were used as control of the SERCA2b immunoreaction, and the β-actin was used as loading control. Quantifications of band intensities showed a significant difference ($p<0.005$, asterisk) in SERCA2b immunostaining in LPS-treated cells compared with untreated cells, that was not observed in the Iba1 immunostaining. Data in C-E are means±SE of three experiments performed in triplicates. Scale bar: 20 µm.

Fig. 3 Inhibition of SERCA stimulates migration in BV2 cells. A. Representative images of scratch assays at the beginning of experiments (0 h) and after 6 h of culture in control (Ctr), 100 ng/ml LPS-containing (LPS) and 100 nM thapsigargin-containing (Tg) medium, before (upper panel) and after washing (lower panel). B. Percentages of occupied areas outside (black bars) and inside (grey bars) the scratch region are represented at 0 h and after 6 h in control medium (LPS- Tg-) and in the presence of LPS (LPS+ Tg-) or thapsigargin (LPS- Tg+), without (6 h) or with washing (6 h + washing). C. Area occupied by cells in the scratch region at different time points (in percentage). D. SERCA2b integrated density of BV2 cells in the scratch assay in control

and thapsigargin conditions at 6 h, compared with control cultures at 0 h. E. Quantification of the number of mitosis per area unit (equivalent to the scratched area in the image), outside (black bars) and inside (grey bars) the scratch region after 6 h with the different treatments (Ctr, LPS, Tg). F. Western blot of the cell proliferation marker PCNA from BV2 extracts treated with LPS or thapsigargin, and adult mouse brain extracts. β-actin was used as loading control. G. Phalloidin staining (green) to visualize actin at different time points of the scratch assay. Cells showed thin filopodia (arrows) at the beginning of the experiment, lamellipodia (arrowheads) after 5 min in both control and thapsigargin conditions. Unlike controls, cells turned to an amoeboid morphology (arrows) after 2 h of thapsigargin treatment. Cell nuclei were visualized with DAPI staining (blue). H. Phalloidin (green) and DAPI (blue) staining of cells outside the scratch after 6 h. Control cells showed thin filopodia while cells treated with thapsigargin exhibited an amoeboid morphology. Data in B, C, D and F are means±SE of three experiments performed in duplicates and asterisks denote significant differences ($p<0.05$) of data compared with their respective controls. Scale bars: 100 μm (A), 5 μm (G, H).

Fig. 4 SERCA2b is overexpressed in microglial primary cultures from mouse brain after LPS activation. A. Double immunofluorescence of SERCA2b (red) and β tubulin (green) in primary microglial cells cultured in control (Ctr) and 100 ng/ml LPS-containing (LPS) medium. Cell nuclei were visualized with DAPI (blue). Localization of SERCA2b was compatible with its presence in the ER and the expected change in cell morphology after microglial activation with LPS was clearly observed. B. Scatter plot showing the distribution of form factor and aspect ratio parameters of control and LPS-activated microglia. C. Integrated density of SERCA2b immunodetection in

control and LPS-activated cells. D and E. Representative Western blots using the anti-SERCA2b (D) and the anti-Iba1 (E) antibodies, with β-tubulin as loading control (left). Quantifications are shown on the right. Data in C-E are means±SE of three experiments performed in triplicates and asterisks denote significant differences ($p<0.005$) of data compared with their respective controls. Scale bar: 20 µm.

Fig. 5 SERCA inhibition stimulates migration in murine primary microglia. A. Representative images (left) of scratch assays at the beginning of experiments (0 h) and after 48 h in control (Ctr), 100 ng/ml LPS-containing (LPS) and 100 nM thapsigargin-containing (Tg) medium, without (upper panel) and after washing (lower panel). Scale bar: 75 µm. The number of cells per area unit (equivalent to the scratched area in the image) outside (black bars) and inside (grey bars) the scratch area are represented in the graph at 0 h and after 48 h in control medium (LPS- Tg-) and in the presence of LPS (LPS+ Tg-) or thapsigargin (LPS- Tg+) before (48 h) or after washing (48 h + washing). B. Numbers of cells per area unit (cells/area) in the scratch at different time points. Data in A and B are means±SE of three experiments performed in duplicates and asterisks denote significant differences ($p<0.005$) of data compared with their respective controls.

Fig. 6 Inhibition of SERCA decreases phagocytosis of latex beads in BV2 cells and primary microglia from mouse brain. A. BV2 cells subjected to the phagocytosis assay using red-fluorescent latex beads. Brightfield image merged with red (beads) and blue (DAPI nuclear staining) channels is shown on the left. On the right, the orthogonal projection obtained by confocal microscopy showed that beads (red) were inside the cell. B. BV2 and primary microglial (Mic) cells subjected to the phagocytosis assay in control (Ctr), 100 ng/ml LPS-containing (LPS) or 100 nM thapsigargin-containing (Tg)

medium. Representative images show merged brightfield and red fluorescent channels and demonstrate moderate, high and scarce phagocytosis of beads in Ctr, LPS and Tg conditions, respectively. Scale bars: 15 µm (A), 20 µm (B, in Ctr and LPS), 50 µm (B, in Tg). C. Percentages of BV2 and microglial cells that did not phagocytose (0, white bars) or phagocytosed few (1-4, gray bars) or many (>5, black bars) beads. Data are means±SE of three experiments performed in triplicates. Asterisks denote significant differences ($p<0.005$) of data compared with their respective controls.

Fig. 7 Inhibition of SERCA decreases phagocytosis of amyloid-β peptide in BV2 cells and primary microglia. A. BV2 cell incubated with oligomeric Aβ peptide whose phagocytosis was detected by immunostaining with anti-Aβ antibody (green). Cell morphology is visualized on the left in a brightfield image merged with images showing anti-β-tubulin (red) immunocytochemistry and DAPI (blue) nuclear staining. On the right, the orthogonal projection obtained by confocal microscopy showed that Aβ (green) was inside the cell. B. Phagocytosis of oligomeric Aβ (green) in BV2 (BV2) and primary microglial (Mic) cells in control (Ctr), 100 ng/ml LPS-containing (LPS) or 100 nM thapsigargin-containing (Tg) medium. Cell morphology and nuclei were visualized by anti-β-tubulin antibody (red) and DAPI (blue), respectively. Scale bars: 15 µm (A), 20 µm (B). C. Quantification of Aβ phagocytosis per cell in terms of integrated density. Data are means±SE of three experiments performed in triplicates. Asterisks denote significant differences ($p<0.05$) of data compared with their respective controls.

Fig. 8 Immunodetection of CD68 in a phagocytosis assay with amyloid-β peptide in BV2 cells. A. BV2 cells were incubated with vehicle (-Aβ) or oligomeric Aβ peptide (+Aβ) in control (Ctr), 100 ng/ml LPS-containing (LPS) or 100 nM thapsigargin-

containing (Tg) medium. Aβ phagocytosis was detected by immunostaining with anti-Aβ antibody (red), CD68 expression with the anti-CD68 antibody (green) and nuclei were visualized by DAPI staining (blue). Scale bar: 25 µm. B. Quantification of CD68 integrated density. Data are means±SE of three experiments performed in triplicates. Asterisks denote significant differences ($p<0.05$) of data compared with their respective controls.

Fig. 9 Presence of Aβ reduces migration in BV2 cells. A. Representative images of scratch assays after 6 h of culture in control (Ctr) or 100 nM thapsigargin-containing (Tg) medium, in the absence (-Aβ) or the presence of oligomeric Aβ peptide (+Aβ). Cells were visualized by DAPI staining. B. Quantification of cells in the scratch region after 6 h of Aβ application revealed less cells in the scratch region in both control and Tg conditions. C. Immunodetection of Aβ phagocytosis (red) in two areas: in the middle of the scratch and at the border of the scratch. The β-tubulin immunodetection (green) and DAPI staining (blue) were used to visualize cell morphology and nuclei, respectively. Migrating cells showed reduced phagocytosis compared with non- or less-migrating cells close to the border of the scratch (arrows). D. Quantification of Aβ-phagocytic cells (in percentage). Data in B and D are means±SE of three experiments performed in triplicates. Asterisks denote significant differences ($p<0.05$) of data compared with their respective controls. Scale bars: 100 µm (A), 50 µm (B).

Figure 1

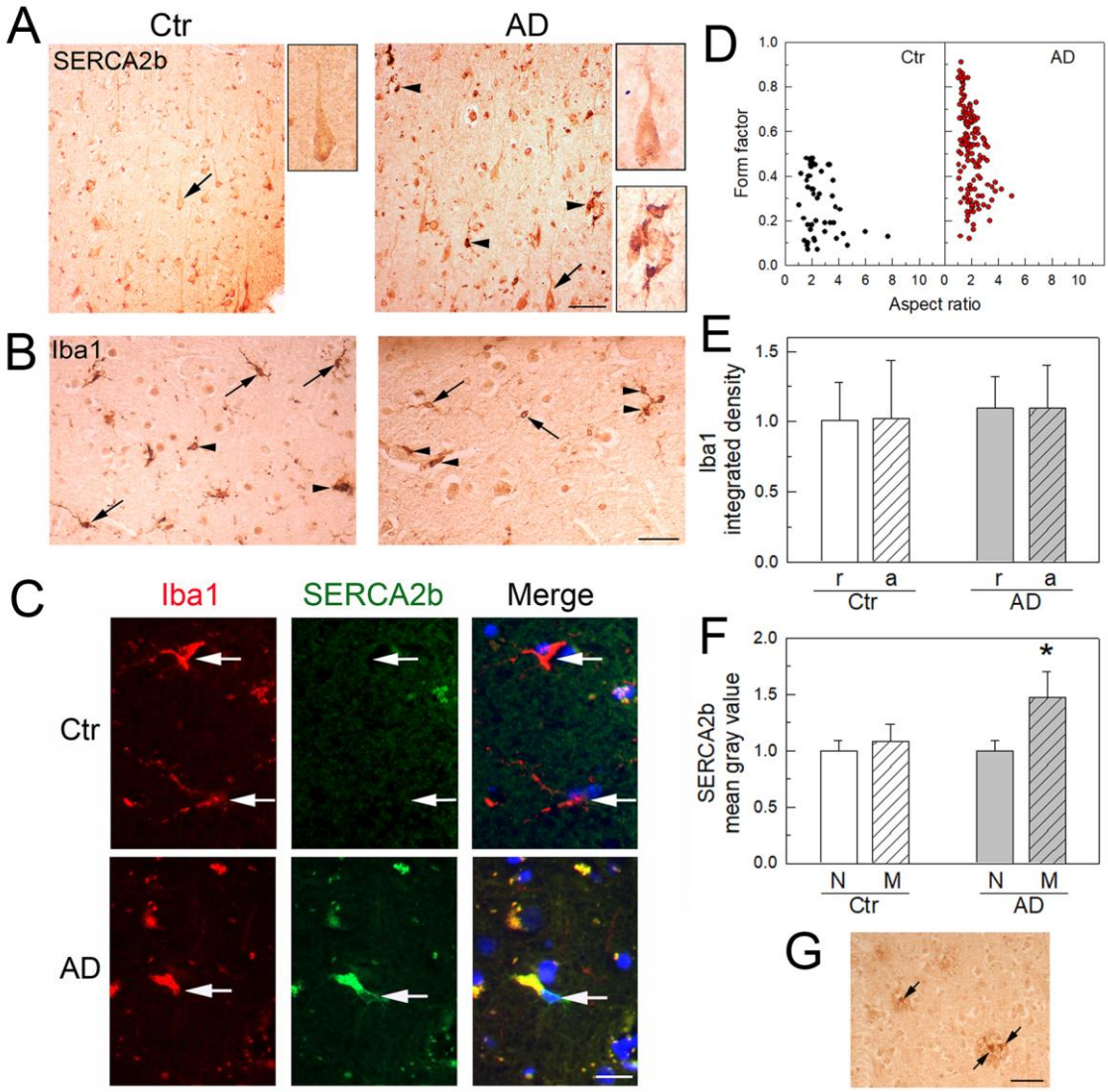
A
Ctr
AD
SERCA2b
B
Iba1
C
Iba1
SERCA2b
Merge
Ctr
AD
D
Ctr
AD
Form factor
Aspect ratio
E
Iba1 integrated density
r a
Ctr
r a
AD
F
SERCA2b mean gray value
*
N M
Ctr
N M
AD
G

Figure 2

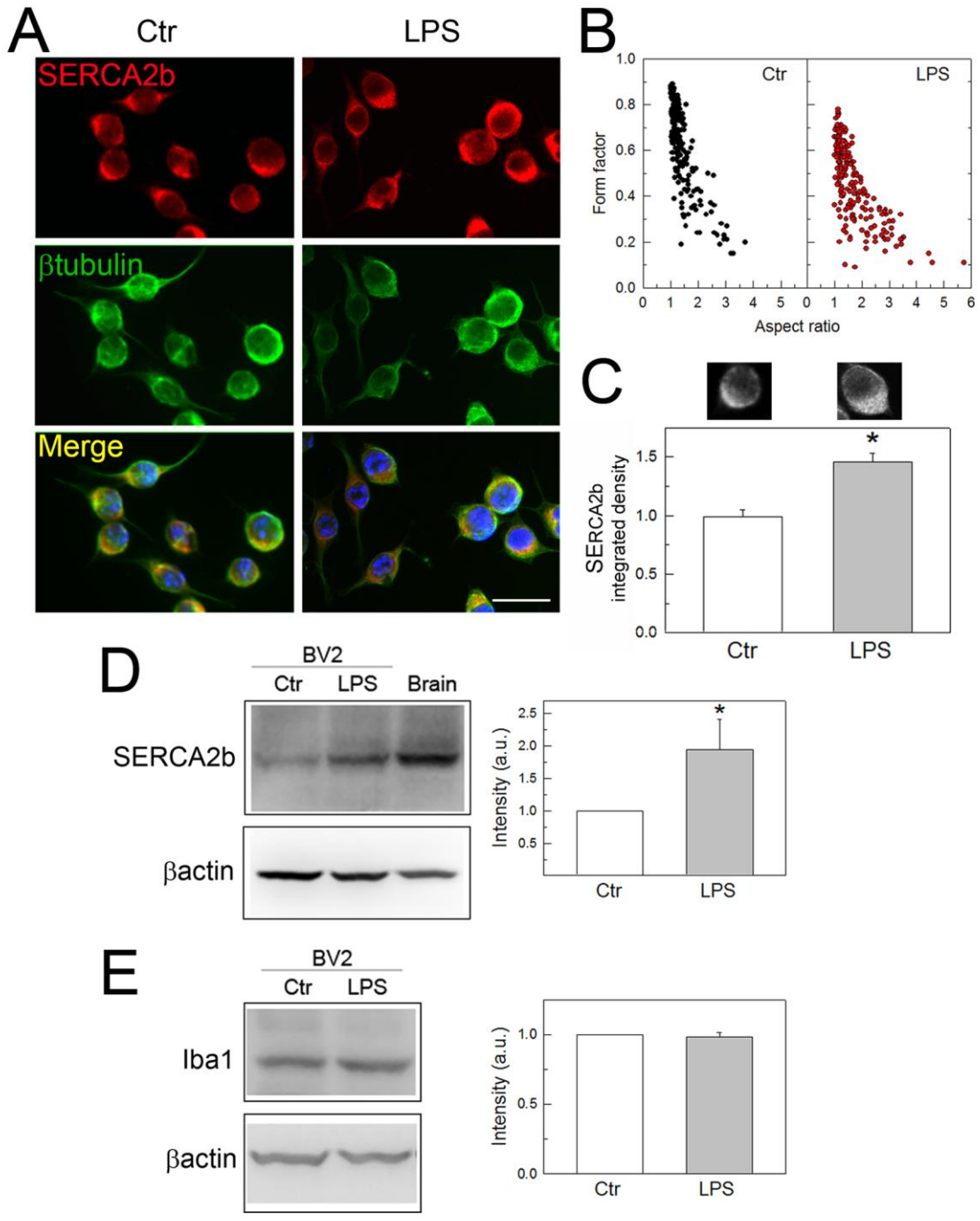
A
Ctr
LPS
SERCA2b
βtubulin
Merge
B
Ctr
LPS
Form factor
Aspect ratio
C
SERCA2b integrated density
Ctr
LPS
D
BV2
Ctr
LPS
Brain
SERCA2b
βactin
Intensity (a.u.)
Ctr
LPS
E
BV2
Ctr
LPS
Iba1
βactin
Intensity (a.u.)
Ctr
LPS

Figure 3

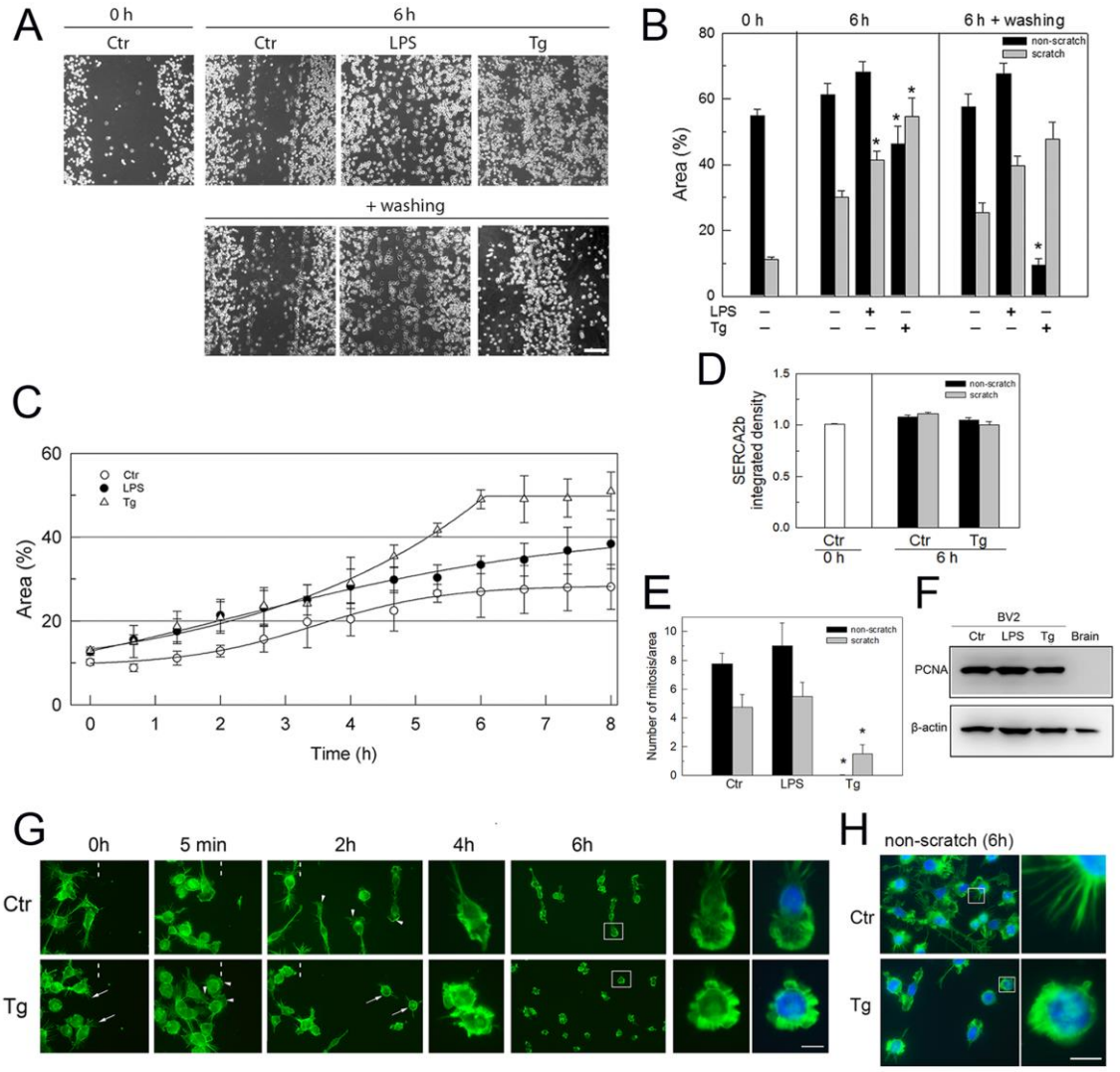
A
0 h
6 h
Ctr
Ctr
LPS
Tg
+ washing
B
0 h
6 h
6 h + washing
non-scratch
scratch
Area (%)
LPS
Tg
C
Ctr
LPS
Tg
Area (%)
Time (h)
D
SERCA2b integrated density
non-scratch
scratch
Ctr
Ctr
Tg
0 h
6 h
E
non-scratch
scratch
Number of mitosis/area
Ctr
LPS
Tg
F
BV2
Ctr
LPS
Tg
Brain
PCNA
β-actin
G
0h
5 min
2h
4h
6h
Ctr
Tg
H
non-scratch (6h)
Ctr
Tg

Figure 4

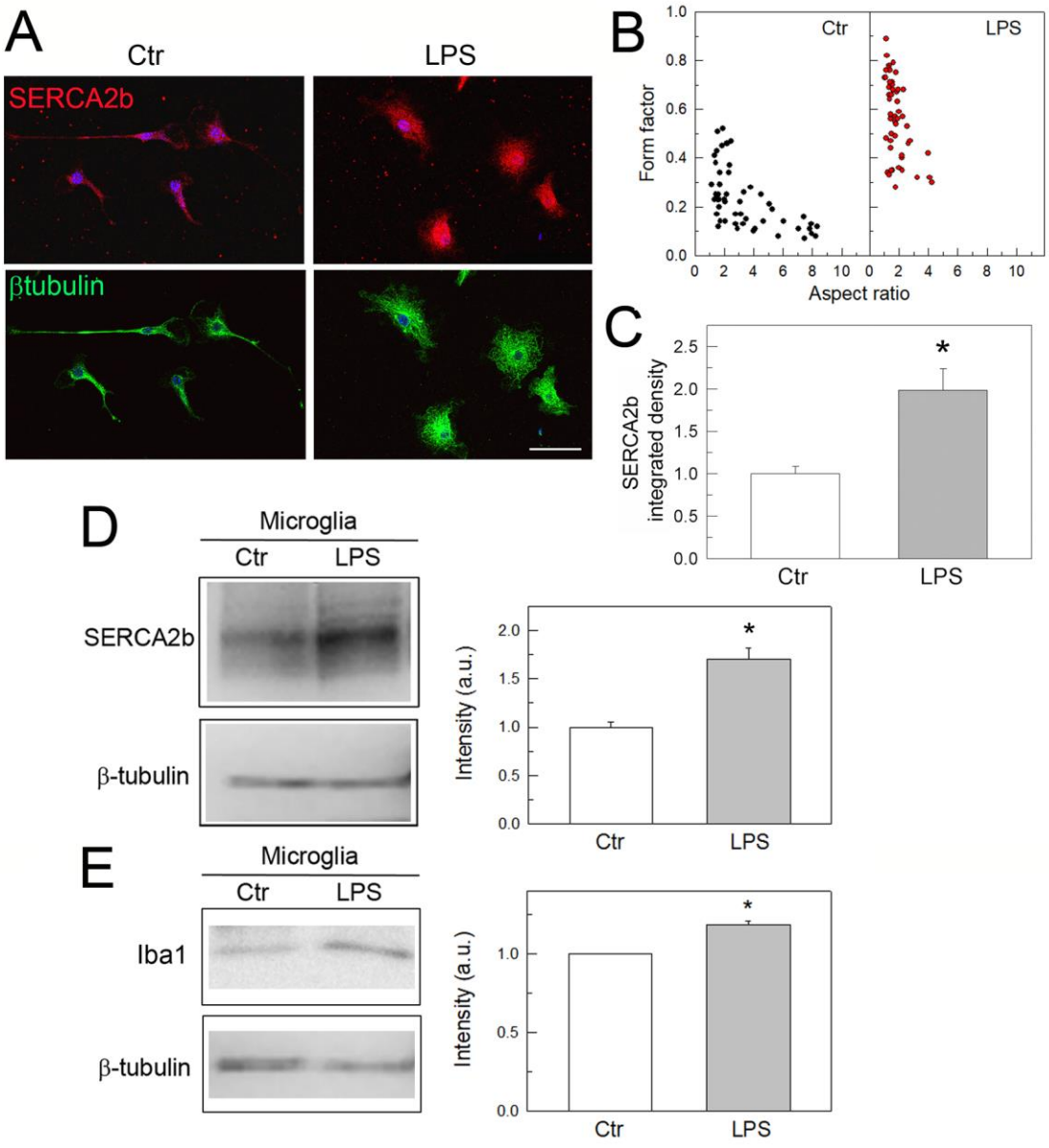
A
Ctr
LPS
SERCA2b
βtubulin
B
Ctr
LPS
Form factor
Aspect ratio
C
SERCA2b integrated density
Ctr
LPS
D
Microglia
Ctr
LPS
SERCA2b
β-tubulin
Intensity (a.u.)
Ctr
LPS
E
Microglia
Ctr
LPS
Iba1
β-tubulin
Intensity (a.u.)
Ctr
LPS

Figure 5

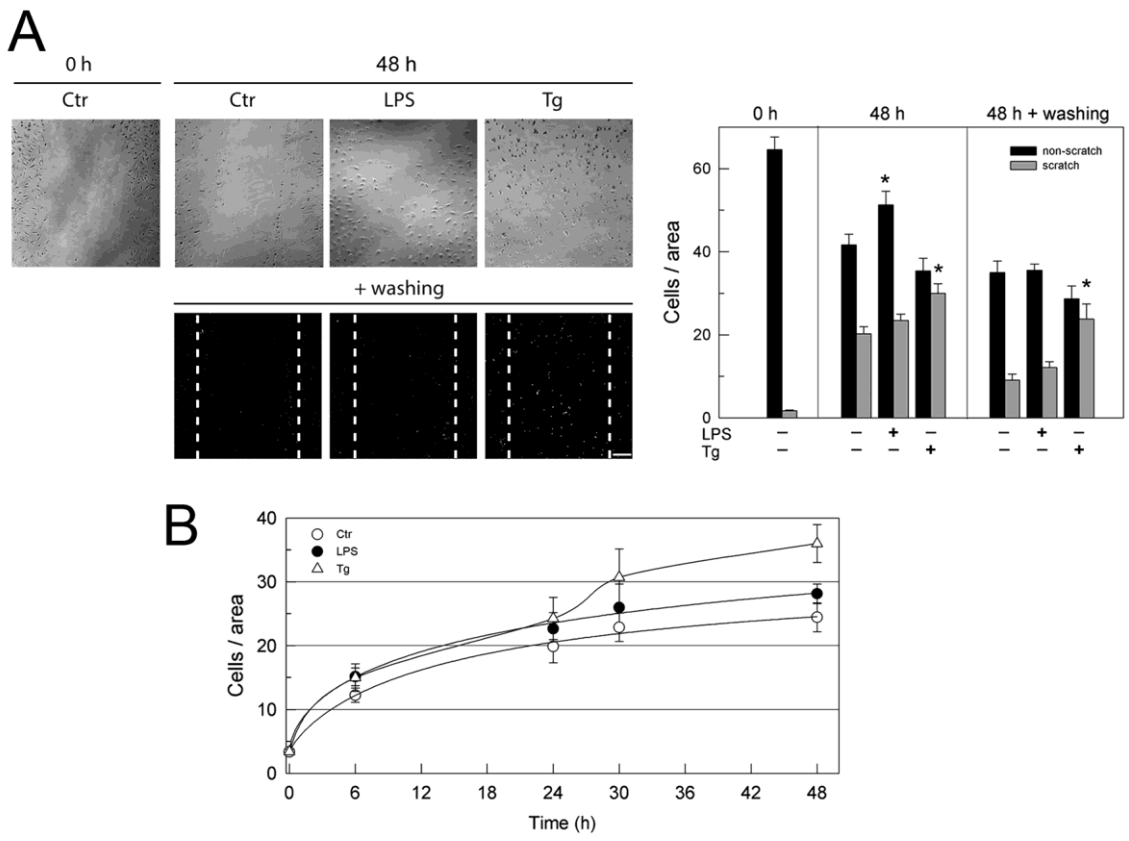
A
0 h
48 h
Ctr
Ctr
LPS
Tg
+ washing
0 h
48 h
48 h + washing
non-scratch
scratch
Cells / area
60
40
20
0
LPS
Tg
B
Ctr
LPS
Tg
Cells / area
40
30
20
10
0
0
6
12
18
24
30
36
42
48
Time (h)

Figure 6

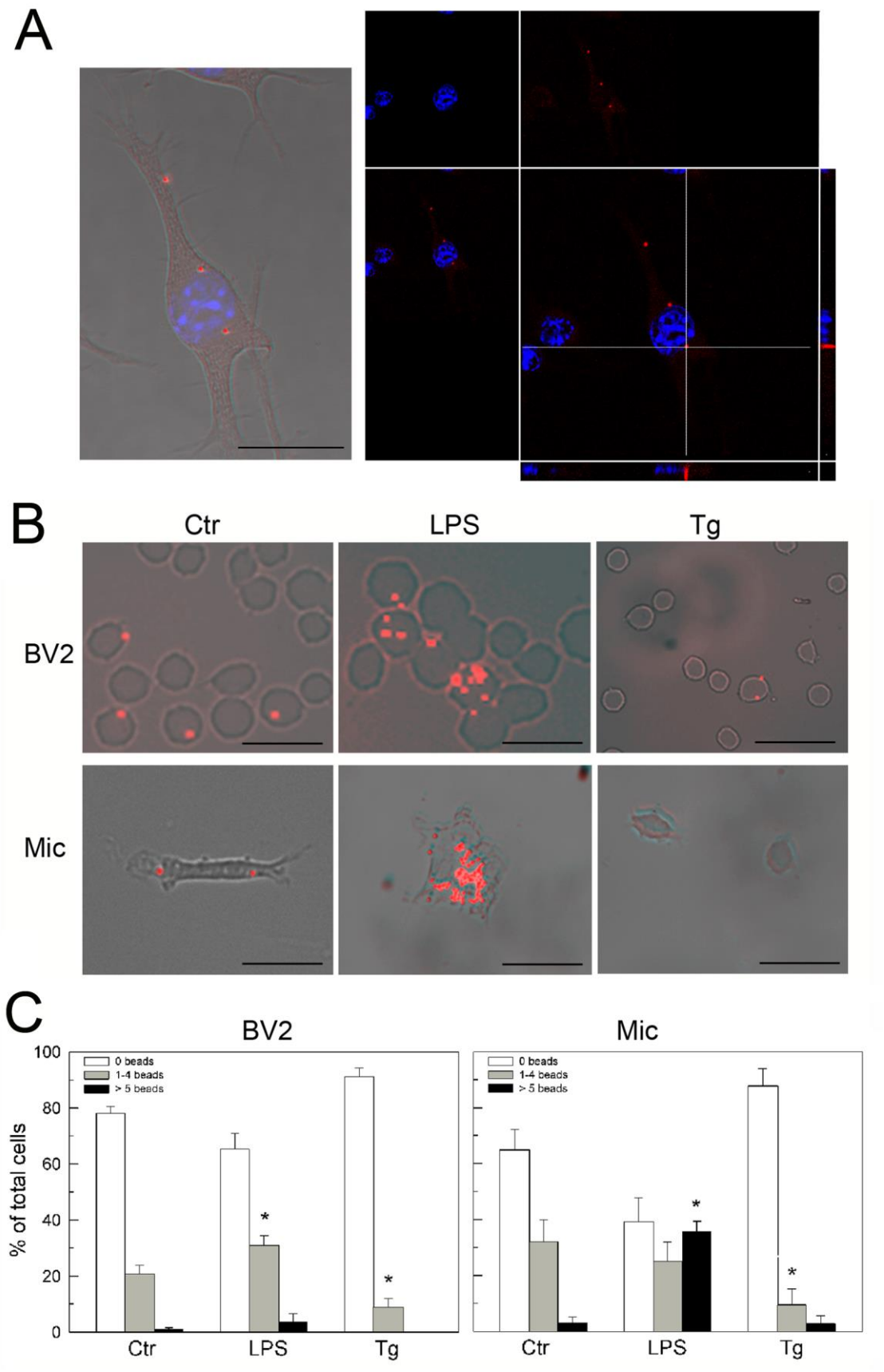
A
B
Ctr
LPS
Tg
BV2
Mic
C
BV2
Mic
0 beads
1-4 beads
> 5 beads
% of total cells
100
80
60
40
20
0
Ctr
LPS
Tg
*

Figure 7

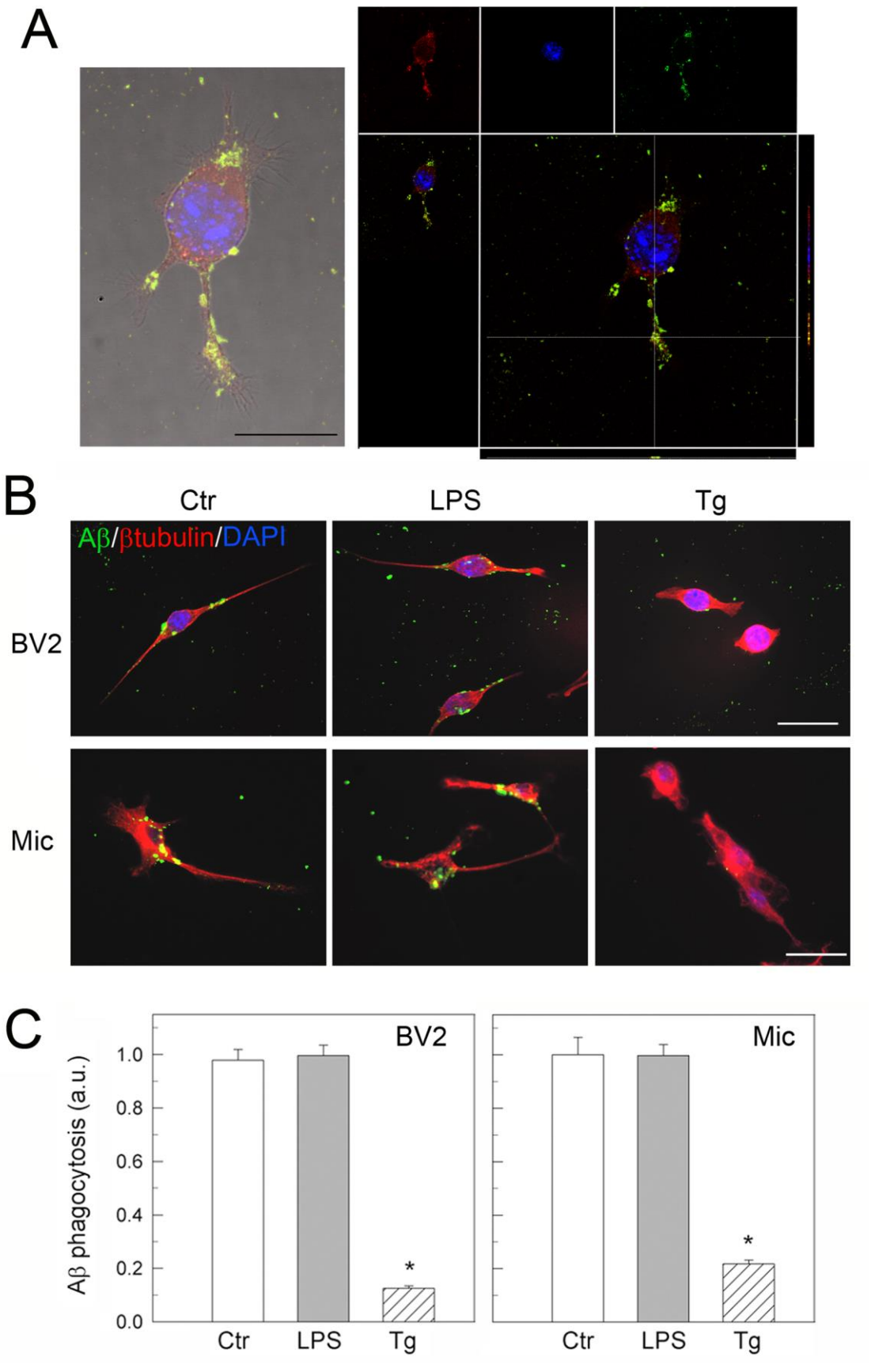
A
B
Ctr
LPS
Tg
Aβ/βtubulin/DAPI
BV2
Mic
C
BV2
Mic
Aβ phagocytosis (a.u.)
1.0
0.8
0.6
0.4
0.2
0.0
*
*
Ctr
LPS
Tg
Ctr
LPS
Tg

Figure 8

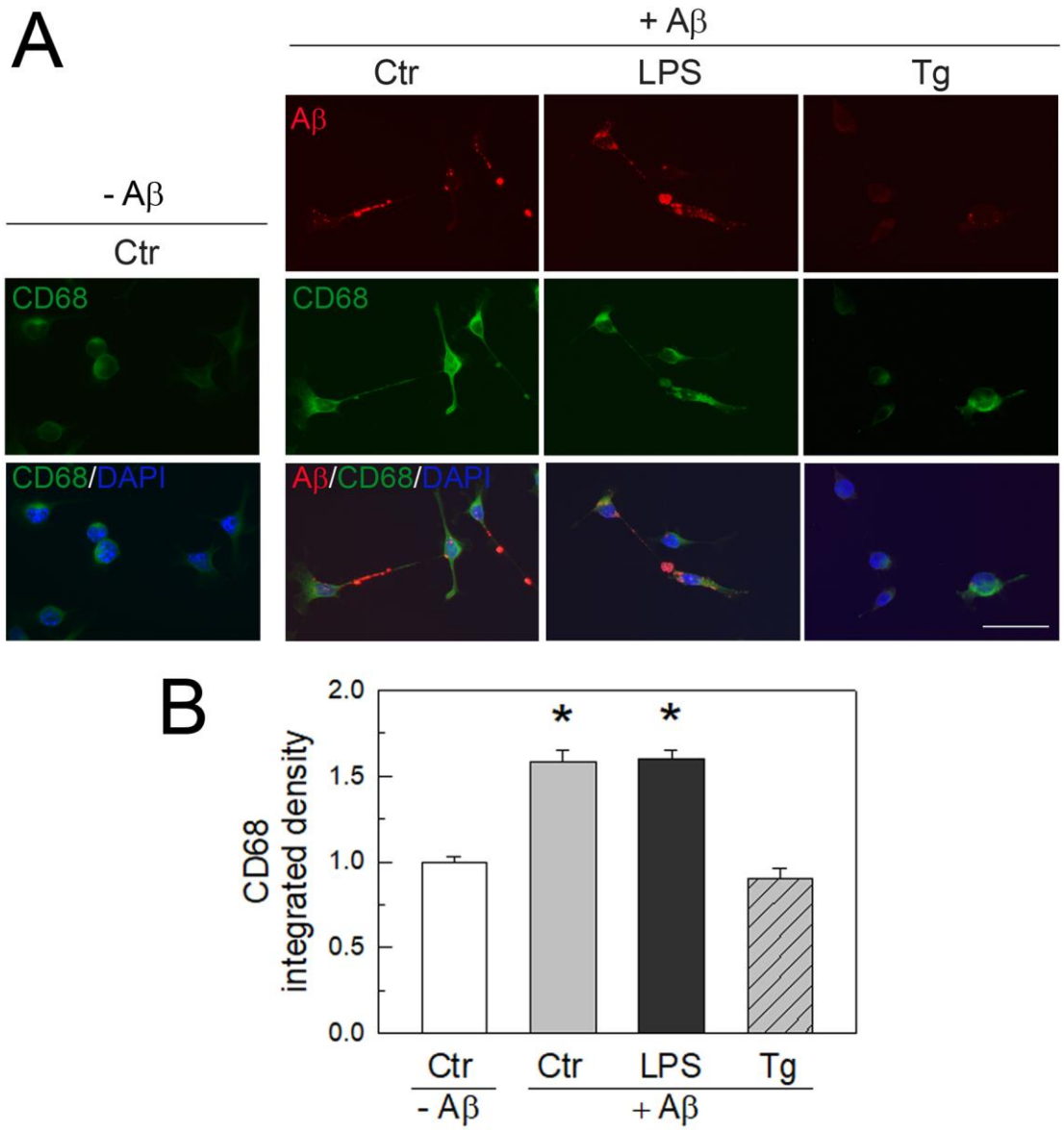
A
+ Aβ
Ctr
LPS
Tg
Aβ
- Aβ
Ctr
CD68
CD68
CD68/DAPI
Aβ/CD68/DAPI
B
CD68 integrated density
2.0
1.5
1.0
0.5
0.0
*
*
Ctr
- Aβ
Ctr
LPS
Tg
+ Aβ

Figure 9

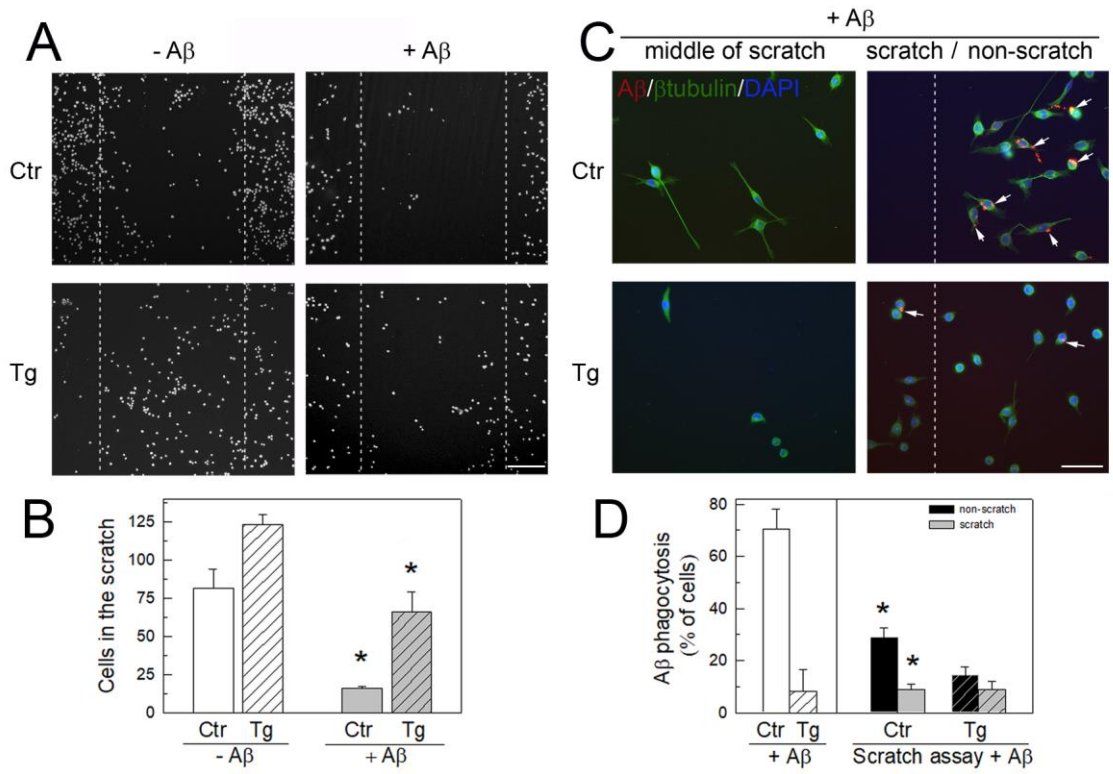
A
- Aβ
+ Aβ
Ctr
Tg
C
+ Aβ
middle of scratch
scratch / non-scratch
Aβ/βtubulin/DAPI
Ctr
Tg
B
Cells in the scratch
125
100
75
50
25
0
Ctr Tg
- Aβ
Ctr Tg
+ Aβ
*
*
D
Aβ phagocytosis
(% of cells)
80
60
40
20
0
non-scratch
scratch
*
*
Ctr Tg
+ Aβ
Ctr Tg
Scratch assay + Aβ